Received: 18 September 2017 | Revised: 8 November 2017 | Accepted: 9 November 2017

DOI: 10.1002/aoc.4222

FULL PAPER

WILEY Applied Organometallic Chemistry

Design, synthesis, pharmacological evaluation and DNA interaction studies of binuclear Pt(II) complexes with pyrazolo[1,5-a]pyrimidine scaffold

Miral V. Lunagariya[1] | Khyati P. Thakor[1] | Bhargav N. Waghela[2] | Chadramani Pathak[2] | Mohan N. Patel[1]

[1]Department of Chemistry, Sardar Patel University, Vallabh Vidyanagar -388 120, Gujarat, India

[2]Department of Cell Biology, School of Biological Sciences and Biotechnology, Indian Institute of Advanced Research, Koba Institutional Area, Gandhinagar 382007, Gujarat, India

Correspondence
Mohan N. Patel, Department of Chemistry, Sardar Patel University, Vallabh Vidyanagar-388 120, Gujarat, India.
Email: jeenen@gmail.com

Substituted pyrazolo[1,5-a]pyrimidine ligands were synthesized by cyclization, using 3-(thiophen-2-yl)-*1H*-pyrazol-5-amine with substituted enones (3-phenyl-1-(pyridin-2-yl)prop-2-en-1-one) in presence of KOH and DMF as solvent to form cyclic aromatic compounds. The substituted pyrazolo[1,5-a] pyrimidine based binuclear Pt^{II} complexes containing neutral tetradentated ligands have general formula $[Pt_2(5a–5f)Cl_4]$, (where, (5a -5f) = pyrazolo[1,5-a] pyrimidine ligand). This compounds were characterized by physicochemical and spectroscopic method like elemental analyses, UV-Visible, FT-IR, EDX, TGA, molar conductivity, magnetic susceptibility measurements, mass spectroscopy, ^{1}H and ^{13}C NMR method. The square planar geometry was predicted by electronic spectral study. All Pt^{II} compounds were evaluated by antimicrobial assay, *in vitro* brine shrimp assay, *in vivo* cellular level bioassay using *S. Pombe* cells and anti-tuberculosis study. LC_{50} (50% lethal concentration) values of compounds are observed between 6.450 - 102.07 μg/mL. UV-vis absorption titration, competitive displacement assay, molecular docking and viscosity measurement were carried out to examine the binding type and binding strength of complexes. The binding studies suggest partial intercalative binding mode of the complexes and the observed binding constant (K_b) values are found in the order of 6d > 6b > 6c > 6a > 6e > 6 f. The anti-proliferative cytotoxicity of the synthesized Pt^{II} complexes (6a-6f) were tested against the HCT-116 (Human Colorectal Carcinoma) cancer cell line.

KEYWORDS
binuclear Pt^{II} complexes, cellular level bioassay, *In vitro* antiproliferation cytotoxicity, pyrazolo[1,5-a] pyrimidine analogous, thermodynamics parameters

1 | INTRODUCTION

Incorporation of fused aza-heterocyclic rings (pyrazole, pyrimidine and pyrazolo[1,5-a]pyrimidine) have been extensively utilized in recent years due to their plethora of applications in a various domains such as medicinal chemistry, organometallics, therapeutic and material chemistry. Five membered aza-heterocyclic molecule, pyrazoles have attained a special status in the eyes of chemists and biologists owing to their easy methods of syntheses and enormous pharmacological applications. Pyrimidine or m-diazine moiety is the parent ring system of a variety of substances which play vital role in biological processes. This structural motif is also subset of a large

number of naturally occurring substances. For example as vitamins, coenzymes, purines, pterins, nucleotides and nucleic acids. The properties of pyrimidines are governed to a large extent by the electron-attracting properties of the two nitrogen atoms; each reinforces the electronic effect of the other in the 2-, 4- and 6-positions. The pyrazolo[1,5-a]pyrimidine motifs are used in medicinal chemistry dealing with antimicrobial anticancer, antitumor, anxiolytic, antimicrobial, antibacterial, antitrichomonal, antischistosomal activities whereas zaleplon, a hypnotic drug; ocinaplon, an anxiolytic drug; pyrazophos, a fungicide, herbicides and insecticide are aspects of pesticide chemistry having a wide range of enzyme inhibitory activities.[1–5]

The platinum-based chemotherapy is currently the most-utilised treatment for cancer, one of the most globally prominent diseases,[6] since the discovery of anti-carcinogenic activity of cisplatin metal-based anticancer drug.[7–9] Other platinum drugs have been developed and marketed, such as carboplatin, oxaliplatin nedaplatin, lobaplatin and heptaplatin, satraplatin and picoplatin.[10] While the second generation of carboplatin, and third generation of oxaplatin, which is more effective and less toxic than cisplatin but possesses the same spectrum of antitumor activity used in combination therapy with 5-fluorouracil for colon cancer.[11]

In bioinorganic chemistry, metal complexes have been used for the treatment of many diseases (cancer, arthritis, diabetes, alzheimer's, etc.), but their mechanism is not completely understood in biological systems[12,13] and their ability to modulate drug metabolism (hydrolysis) and target binding through steric and electronic effects on the substitution mechanism worldwide efforts are made to develop platinum-based anticancer agents. The electron-rich nature of biomolecular (DNA) and electron-deficient metal ions are believed to have strong interactions, which are thought to be the criteria for the pharmaceutical activities of the complexes. DNA plays a central role in replication, transcription and regulation of genes as an important target of anticancer drugs. The existence of metal-binding sites in the DNA structure makes different types of interaction possible. It has been reported that the metal complexes can interact with DNA non-covalently in the mode of intercalation, groove binding and electrostatic effect.[14,15] The insertion of biologically-active ligands into metal coordination compounds have much scope for the design of novel drugs with improved and targeted activity. Studies on such complexes indicate that new mechanisms of action are favourable when combining the bioactivity of the ligand with the properties inherent to the metal, leading to the possibility of overcoming the current drug resistance pathways.

Ligands can be introduced into a system to limit the adverse effects of excess metal ions. Upon chelation of ligands to the metal ion, some drastic changes occurred, which includes increased lipophilicity, stabilizing specific oxidation states and contributing to substitution inertness. As an alternative, many platinum complexes with π-conjugated heterocyclic ligands have been developed and their anti-cancer curing properties are investigated. Precisely designed ligands for metal-based medicinal agents can play an integral role in achieving the potential toxicity of a metallo drug, which can be used for diagnosis and therapy.

In current work, we have concentrated on following points: (a) synthesis of ligands (5a-5f) by two step reaction employing conventional method and synthesis of target binuclear Pt^{II} complexes (6a-6f) by single step one-pot two-component (b) biological evaluation including DNA binding studies, DNA nuclease, antibacterial, antituberculosis studies, *in vitro* cytotoxicity against *S. pombe* cellular level and brine shrimp lethality assay. In the framework of biological importance, we intended to develop new approach for structural diversity of heterocycles incorporating scaffold. The modifications made on pyrazolo[1,5-a]pyrimidine centre for probing antibacterial, antitubercular activity includes; (A) thiophene ring at C-3 position (B) 4-substituted phenyl nucleus at C-8 position and (C) pyridine group on C-6 position to validate lipophilicity of the target molecules (6a-6f). All synthesized compounds were evaluated for their biological applications. Based on the assessment of these inspections and the persistence of the research work on bioactive heterocycles, their design and potential applications are anticipated.

2 | EXPERIMENTAL

2.1 | Materials and reagents

All the commercial analytical grade reagents, solvents and chemicals (> 95 % purity) were used without further purification and purchased from Sigma Aldrich Chemical Co. (Vadodara, India). K_2PtCl_4 salts was purchased from S. D Fine-Chem Ltd. (SDFCL). Herring sperm (HS) DNA, 3-(thiophen-2-yl)-1H-pyrazol-5-amine, 4-methoxy benzaldehyde, 4-fluoro benzaldehyde, 4-chloro benzaldehyde, 4-nitro benzaldehyde, 4-methyl benzaldehyde and 2-acetyl pyridine were purchased from Sigma Aldrich Chemical Co. (India). All the bacterial cultures used were purchased from MTCC, Institute of Microbial Technology and Chandigarh, India. An *Artemia cyst* was purchased from local aquarium store. Nutrient broth (NB), agarose, ethidium bromide (EtBr), tris-acetyl-EDTA (TAE), bromophenol blue was purchased from Himedia (India).

Thin layer chromatography (TLC) was performed using Merck aluminium sheets coated with silica gel plates (silica gel 60 F_{254} 0.25 mm). Purification by flash chromatography was performed using Merck silica gel 60. and components were visualized by observation under UV light. GenElute mini Pre Kit for pUC19 DNA isolation was purchased from Sigma Aldrich (India). *S. pombe* Var. Paul Linder 3360 was obtained from IMTECH, Chandigarh, India. MilliQ™ (18.2 m℧, Millipore) was used for the preparation of all deionized water. HPLC grade DMSO was used to dissolve the platinum compounds.

2.2 | Physical measurements

^{1}H NMR and ^{13}C NMR spectra were obtained on a 400 and 100 MHz, Bruker Avance nuclear magnetic resonance spectrometer, either in D_2O (25 °C) or DMSO-d_6 (35 °C), and TMS as the internal reference. The following abbreviations apply to splitting patterns: s (singlet), d (doublet), t (triplet), q (quartet), m (multiplet). The chemical shift (parts per million) of each resonance were repeated as an approximate midpoint of its multiplicity, δ (ppm) and the coupling constants (J) in Hz. The attached proton test in a ^{13}C NMR characterisation showed C, CH, CH_2 and CH_3 signals unattached to protons. The APT experiment yields methine (CH) and methyl (CH_3) signals negative and quaternary (C) and methylene (CH_2) signals positive. Infrared spectra were recorded on a FT-IR ABB Bomen MB-3000 spectrophotometer (Canada) in the range of 4,000 to 400 cm^{-1}.

Elemental analysis C, H, N and S of the synthesized compounds was performed with a model Euro EA elemental analyser. Melting points (^{0}C, uncorrected) were determined in open capillaries on thermoCal10 melting point apparatus (Analab Scientific Pvt. Ltd, Vadodara, India). The mass spectra were obtained on a Thermo scientific mass spectrophotometer (USA), using the positive electrospray ionisation mode. The electronic spectra were recorded on a UV-160A UV-vis spectrophotometer (Shimadzu, Kyoto, Japan). The magnetic moments were measured by Gouy's method using mercury tetrathiocyanatocobaltate(II) as the calibrate (χ_g = 16.44×10^{-6} cgs units at 20 °C) citizen balance. Antibacterial study was carried out by means of laminar airflow cabinet (Toshiba, Delhi, India). The thermo gram of complexes was recorded with a Mettler Toledo TGA Thermogravimetric analyser. Fluorescence spectroscopy was carried out by FluoroMax-4, spectrofluorometer, HORIBA (Scientific). Conductance measurement was carried out using conductivity meter model number E-660A. Photo quantization of the gel after electrophoresis was done using AlphaDigiDocTM RT. Version V.4.0.0 PC-Image software, CA, USA).

2.3 | General synthesis of ligands and complexes

2.3.1 | Claisen-Schmidt condensation reaction (3a-3f)

The α, β unsaturated carbonyl compounds derived by this method.[16] Compounds (3a-3f) were obtained after stirring at room temperature for 2 h a solution containing (1.241 g, 1 mmol) 1-(pyridin-2-yl)ethan-1-one (1a), in 10 ml methanol and KOH (0.673 g, 1.2 mmol, 20 ml) was added as a catalytic amount Claisen-Schmidt condensation reaction, with appropriately *P*-substituted benzaldehyde (-OCH_3, -F, Cl, -NO_2, -CH_3, -H 1 mmol) (2a-2f) was added drop wise into the reaction mixture. The reaction mixture was cooled on an ice bath and neutralized with dilute hydrochloric acid. The crude material appeared was separated by suction pump and washed with water-methanol 50% system (60 ml × 3). The solvent was removed under reduced pressure. The obtained material was recrystallized from methanol. The purity of the products was checked on TLC by using mixture of (ethylacetate: hexane, 4:1) system. The solvent was removed under reduced pressure to smoothly afford the corresponding chalcones as a white solid. The proposed reaction scheme for the synthesis of chalcone (3a-3f) is shown in Scheme 1.

2.4 | General procedure for the preparation of pyrazolo[1,5-a]-pyrimidines chimeras (5a-5f)

Lipson and co-workers reported synthesis of the pyrazolo[1,5-a]pyrimidines derivatives method.[17–19] Chalcones (3a-3f) are effective bidentate electrophiles and have been employed for the synthesis of various bioactive heterocyclic. To the solution of the appropriate enones (3a-3f) (0.50 g, 2.8 mmol) in 10 ml of DMF, 3-(thiophen-2-yl)-1H-pyrazol-5-amine (4a) (0.33 g, 3.0 mmol) and KOH (0.0056 g, 0.1 mmol) solution were added, the reaction mixture was refluxed for 30 min. Upon completion of reaction as indicated by TLC plates, the excess of solvent was removed under reduced pressure and the reaction mixture was cooled on an ice bath. The reaction mixture was extracted with ethylacetate (50 ml × 3), washed thoroughly with water (30 ml × 3), added brine solution of sodium chloride and dried over sodium sulphate. The resulting mixture was concentrated under vacuum. The residue was purified by chromatography on silica gel system (ethylacetate: hexane, 4:1) to obtain the pyrazolo[1,5-a]pyrimidine chimera product. The proposed reaction scheme for the synthesis of ligands (5a-5f) is shown in Scheme 1. ^{1}H NMR, ^{13}C NMR spectra

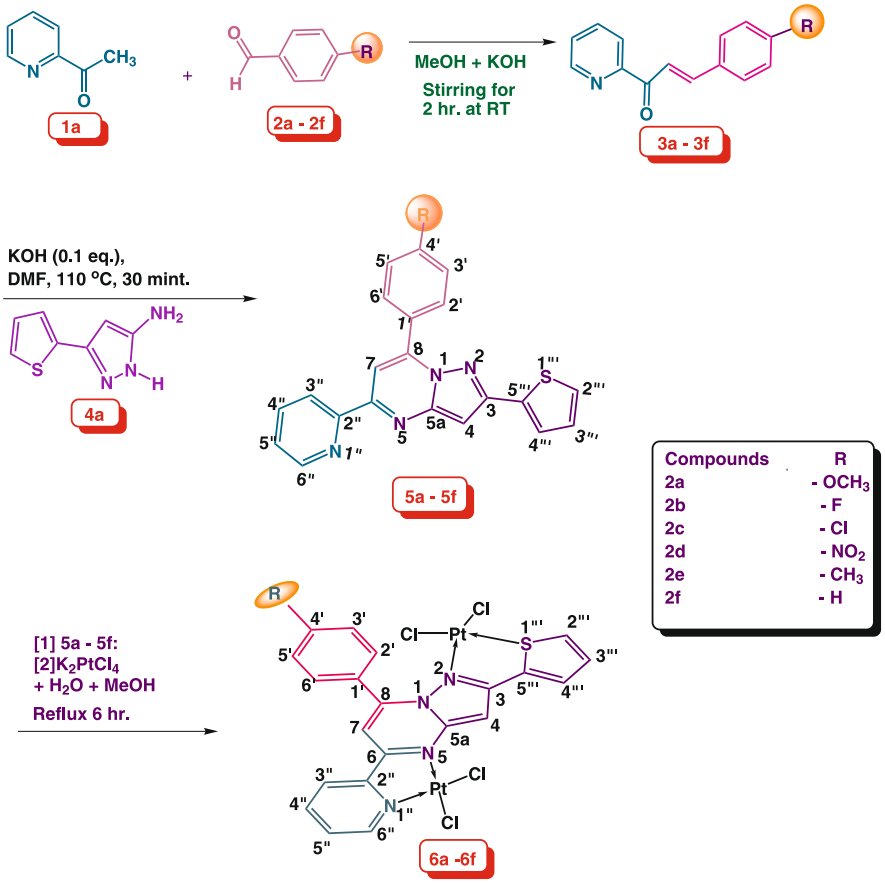

SCHEME 1 Synthesis of chalcone (3a-3f), pyrazolo[1,5-a] pyrimidine derivatives ligands (5a–5f) coordinated to Pt^{II} metal ions to give complexes (6a-6f) and numbering scheme of atoms

of ligands are shown in supplementary material 1 and 2, respectively.

2.4.1 | 7-(4-Methoxyphenyl)-5-(pyridin-2-yl)-2-(thiophen-2-yl)pyrazolo[1,5-a] pyrimidine (5a)

It was synthesized using chalcone (*E*)-3-(4-methoxyphenyl)-1-(pyridin-2-yl)prop-2-en-1-one **(3a)** (0.333 g, 2.8 mmol) and 3-(thiophene-2-yl)-1*H*-pyrazol-5-amine **(4a)** (0.50 g, 3.0 mmol) as described in general process. Colour: light yellow crystal, Yield: 82 %, mol. wt. 384.46 g/mol, m.p. 233 °C; Anal. Calc. (%) For $C_{22}H_{16}N_4OS$: C, 68.73; H, 4.20; N, 14.57; S, 8.34. Found (%): C, 68.98; H, 3.92; N, 14.39; S, 8.02. UV-vis: λ (nm) (ε, M^{-1} cm^{-1}): 309 (39,650), 358 (26,830). ^{1}H NMR (400 MHz, DMSO-d_6) δ/ppm: 8.752 (d, 1H, J= 8.0 Hz, $H_{2'''}$), 8.582 (d, 1H, J= 7.6 Hz, $H_{4'''}$), 8.365 (d, 2H, J= 8.0 Hz, $H_{2',6'}$), 8.160 (s, 1H, H_7), 7.911(t, 1H, $^3J_1$= 8.0 Hz, $^3J_2$= 8.4 Hz, $H_{3'''}$), 7.629 (dd, 2H, $^3J_1$= 2.4 Hz, $^4J_2$= 6.8 Hz, $H_{3'',6''}$), 7.396 (t, 1H, $^3J_1$= 7.6 Hz, $^3J_2$= 8.0 Hz, $H_{5''}$), 7.167 - 7.120 (multiplet, 3H, $H_{3',5',4''}$), 7.008 (s, 1H, H_4), 3.957 (s, 3H, -OCH_3). ^{13}C NMR (100 MHz, DMSO-d_6) δ/ppm: 165.23 ($C_{quat.}$, C_6), 160.63 ($C_{quat.}$, O-CH_3), 155.23 ($C_{quat.}$, $C_{2''}$), 154.73 ($C_{quat.}$, C_{5a}), 149.98 (CH, $C_{6''}$), 147.51 ($C_{quat.}$, C_8), 139.91 ($C_{quat.}$, $C_{5'''}$), 137.19 (CH, $C_{4''}$), 136.42 ($C_{quat.}$, C_3), 131.83 (CH, $C_{4''}$), 128.63 (CH, $C_{2'''}$), 128.44 (CH, $C_{2'}$, $C_{6'}$), 128.0 (CH, $C_{3'''}$), 125.38 ($C_{quat.}$, $C_{1'}$), 123.55 (CH, $C_{5''}$), 121.60 (CH, $C_{3''}$), 114.85 (CH, $C_{3'}$, $C_{5'}$), 105.97 (CH, C_7), 93.5 (CH, C_4), 55.8 (O-CH_3). [Total signal observed = 20: signal of C and CH_2 = 8 (Ar-C = 2, pyridine-C = 1, thiophene-C = 1, pyrazolo[1,5-a]pyrimidine-C = 4), signal of CH and CH_3 = 12 (Ar-CH = 2, pyridine-CH = 4, thiophene-CH = 3, pyrazolo[1,5-a] pyrimidine-CH = 2), O-CH_3 = 1]. FT-IR: (KBr pellet) ν_{max} (cm^{-1}): 3109 $\nu_{(=C-H)ar}$ (w), 1604 $\nu_{(C=N)}$ (s), 1458 – 1566 $\nu_{(C-H)banding}$ (s), 1257 $\nu_{(C-C)alkanes}$ (s), 1650 $\nu_{(C=C)conjugated\ alkenes}$ (w), 1026 $\nu_{(C-S-C)stre.\ (thiophene\ ring)}$ (s), 709 – 833 $\nu_{(Ar\ -\ H)2\ adjacent\ hydrogen}$ (s), 586 $\nu_{(=C-H)oop\ band}$ (s). Mass (m/z): 385 $[M]^+$.

2.4.2 | 7-(4-Fluorophenyl)-5-(pyridin-2-yl)-2-(thiophen-2 yl)pyrazolo[1,5-a]pyrimidine (5b)

It was synthesized using chalcone (*E*)-3-(4-fluorophenyl)-1-(pyridin-2-yl)prop-2-en-1-one **(3b)** (0.299 g, 2.8 mmol) and 3-(thiophene-2-yl)-1*H*-pyrazol-5-amine **(4a)** (0.50 g, 3.0 mmol) as described in general process. Colour: yellow crystal, Yield: 85 %, mol. wt. 372.42 gm/mol, m.p. 223 °C; Chemical formula: $C_{21}H_{13}FN_4S$; UV-vis: λ (nm) (ε, M^{-1} cm^{-1}): 294 (36,740), 357 (7,960). ^{1}H NMR (400 MHz,

DMSO-d_6) δ/ppm: 8.789 (d, 1H, J= 8.0 Hz, $H_{2'''}$), 8.427 (d, 1H, J= 8.0 Hz, $H_{4'''}$), 8.283 (d, 2H, J= 8.8 Hz, $H_{2',6'}$), 8.127 (s, 1H, H_7), 8.079 (t, 1H, $^3J_1$= 8.0 Hz, $^3J_2$= 8.8 Hz, $H_{3'''}$), 7.787 (d, 1H, J= 8.0 Hz, $H_{3'}$), 7.763 (d, 1H, J= 7.2 Hz, $H_{5'}$), 7.668 (t, 1H, $^3J_1$= 5.2 Hz, $^3J_2$= 5.6 Hz, $H_{5''}$), 7.576 (dd, 2H, $^3J_1$= 8.0 Hz, $^4J_2$= 3.6 Hz, $H_{3'',6''}$), 7.347 (s, 1H, H_4), 7.212 (t, 1H, $^3J_1$= 7.6 Hz, $^3J_2$= 7.6 Hz, $H_{4''}$). ^{13}C NMR (100 MHz, DMSO-d_6) δ/ppm: 165.35 ($C_{quat.}$, C_6), 162.60 ($C_{quat.}$, $C_{4'}$), 155.03 ($C_{quat.}$, $C_{2''}$), 154.43 ($C_{quat.}$, C_{5a}), 149.18 (CH, $C_{6''}$), 147.21 ($C_{quat.}$, C_8), 139.44 ($C_{quat.}$, $C_{5'''}$), 137.30 (CH, $C_{4''}$), 136.42 ($C_{quat.}$, C_3), 131.73 (CH, $C_{4''}$), 130.6 (CH, $C_{2'}$, $C_{6'}$), 128.44 (CH, $C_{2'''}$), 128.0 (CH, $C_{3'''}$), 125.20 ($C_{quat.}$, $C_{1'}$), 123.87 (CH, $C_{5''}$), 121.29 (CH, $C_{3''}$), 116.85 (CH, $C_{3'}$, $C_{5'}$), 105.07 (CH, C_7), 93.15 (CH, C_4). [Total signal observed = 19: signal of C and CH_2 = 8 (Ar-C = 2, pyridine-C = 1, thiophene-C = 1, pyrazolo[1,5-a]pyrimidine-C = 4), signal of CH and CH_3 = 11 (Ar-CH = 2, pyridine-CH = 4, thiophene-CH = 3, pyrazolo[1,5-a]pyrimidine-CH = 2)]. FT-IR: (KBr pellet) ν_{max} (cm^{-1}): 3102 $\nu_{(=C-H)ar}$ (w), 1704 $\nu_{(C=N)}$ (s), 1612 $\nu_{(C=C)conjugated\ alkenes}$ (s), 1496 – 1566 $\nu_{(C-H)banding}$ (s), 1218 $\nu_{(C-C)alkanes}$ (s), 1149 $\nu_{(Ar-F)}$ (s), 1056 $\nu_{(C-S-C)stre.\ (thiophene\ ring)}$ (m), 709 – 840 $\nu_{(Ar-H)2\ adjacent\ hydrogen}$ (s), 586 $\nu_{(=C-H)oop\ band}$ (s). Mass (m/z): 373 $[M]^+$.

2.4.3 | 7-(4-Chlorophenyl)-5-(pyridin-2-yl)-2-(thiophen-2 yl)pyrazolo[1,5-a] pyrimidine (5c)

It was synthesized using chalcone (*E*)-3-(4-chlorophenyl)-1-(pyridin-2-yl)prop-2-en-1-one **(3c)** (0.345 g, 2.8 mmol) and 3-(thiophene-2-yl)-1*H*-pyrazol-5-amine **(4a)** (0.50 g, 3.0 mmol) as described in general process. Colour: yellow crystal, Yield: 83 %, mol. wt. 388.87 gm/mol, m.p. 226 °C; Anal. Calc. (%) For $C_{21}H_{13}ClN_4S$: C, 64.86; H, 3.37; N, 14.41; S, 8.24. Found (%): C, 64.58; H, 2.99; N, 13.97; S, 8.00. UV-vis: λ (nm) (ε, M^{-1} cm^{-1}): 283 (40,000), 359 (12,480). ^{1}H NMR (400 MHz, DMSO-d_6) δ/ppm: 8.789 (d, 1H, J= 7.6 Hz, $H_{2'''}$), 8.529 (d, 1H, J= 7.6 Hz, $H_{4'''}$), 8.342 (d, 2H, J= 6.8 Hz, $H_{2',6'}$), 8.113 (s, 1H, H_7), 8.080 (t, 1H, $^3J_1$= 9.2 Hz, $^3J_2$= 7.6 Hz, $H_{3'''}$), 7.790 (d, 1H, J= 8.4 Hz, $H_{3'}$), 7.660 (d, 1H, J= 8.0 Hz, $H_{5'}$), 7.647 (t, 1H, $^3J_1$= 8.0 Hz, $^3J_2$= 8.4 Hz, $H_{5''}$), 7.551 (dd, 2H, $^3J_1$= 8.8 Hz, $^4J_2$= 4.8 Hz, $H_{3'',6''}$), 7.341(s, 1H, H_4), 7.230 (t, 1H, $^3J_1$= 7.6 Hz, $^3J_2$= 8.0 Hz, $H_{4''}$). ^{13}C NMR (100 MHz, DMSO-d_6) δ/ppm: 165.27 ($C_{quat.}$, C_6), 155.30 ($C_{quat.}$, $C_{2''}$), 154.89 ($C_{quat.}$, C_{5a}), 149.20 (CH, $C_{6''}$), 147.34 ($C_{quat.}$, C_8), 139.91 ($C_{quat.}$, $C_{5'''}$), 137.49 (CH, $C_{4''}$), 136.87 ($C_{quat.}$, C_3), 134.30 ($C_{quat.}$, $C_{4'}$), 131.90 (CH, $C_{4'''}$), 131.10 ($C_{quat.}$, $C_{1'}$), 129.44 (CH, $C_{3',5'}$), 128.90 (CH, $C_{2',6'}$), 128.60 (CH, $C_{2'''}$), 128.00 (CH, $C_{3'''}$), 123.29 (CH, $C_{5''}$), 121.40 (CH, $C_{3''}$), 105.09 (CH, C_7), 93.05 (CH, C_4). [Total signal observed = 19: signal of C and CH_2 = 8 (Ar-C = 2, pyridine-C = 1, thiophene-C = 1, pyrazolo[1,5-a]pyrimidine-C = 4), signal of CH and CH_3 = 11 (Ar-CH = 2, pyridine-CH = 4, thiophene-CH = 3, pyrazolo[1,5-a]pyrimidine-CH = 2)]. FT-IR: (KBr pellet) ν_{max} (cm^{-1}): 3101 $\nu_{(=C-H)ar}$ (w), 1704 $\nu_{(C=N)}$ (s), 1612 $\nu_{(C=C)conjugated\ alkene}$ (s), 1496 – 1566 $\nu_{(C-H)banding}$ (s), 1218 $\nu_{(C-C)alkanes}$ (s), 1141 $\nu_{(Ar\ -Cl)}$ (m), 1080 $\nu_{(C-S-C)stre.\ (thiophene\ ring)}$ (s), 709 – 833 $\nu_{(Ar-H)2\ adjacent\ hydrogen}$ (s), 586 $\nu_{(=C-H)oop\ band}$ (s). Mass (m/z): 389 $[M]^+$, 390 [M+2].

2.4.4 | 7-(4-Nitrophenyl)-5-(pyridin-2-yl)-2-(thiophen-2-yl)pyrazolo[1,5-a]pyrimidine (5d)

It was synthesized using chalcone (*E*)-3-(4-nitrophenyl)-1-(pyridin-2-yl)prop-2-en-1-one **(3d)** (0.375 g, 2.8 mmol) and 3-(thiophene-2-yl)-1*H*-pyrazol-5-amine **(4a)** (0.50 g, 3.0 mmol) as described in general process. Colour: brown powder, Yield: 88 %, mol. wt. 399.43 gm/mol, m.p. 224 °C; Anal. Calc. (%) For $C_{21}H_{13}N_5O_2S$: C, 63.15; H, 3.28; N, 17.53; S, 8.03. Found (%): C 63.09; H, 3.30; N, 17.48; S, 7.95. UV-Vis: λ (nm) (ε, M^{-1} cm^{-1}): 294 (32,660), 359 (6,280). ^{1}H NMR (400 MHz, DMSO-d_6) δ/ppm: 8.755 (d, 1H, J= 8.0 Hz, $H_{2'''}$), 8.512 (d, 1H, J= 8.0 Hz, $H_{4'''}$), 8.329 (d, 2H, J= 9.2 Hz, $H_{3',5'}$), 8.097 (s, 1H, H_7), 8.053 (t, 1H, $^3J_1$= 7.6 Hz, $^3J_2$= 7.6 Hz, $H_{3'''}$), 7.778 (d, 1H, J= 7.2 Hz, $H_{2'}$), 7.651 (d, 1H, J= 7.6 Hz, $H_{6'}$) 7.551 (t, 1H, $^3J_1$= 8.0 Hz, $^3J_2$= 8.0 Hz, $H_{5''}$), 7.506 (dd, 2H, $^3J_1$= 9.2 Hz, $^4J_2$= 4.0 Hz, $H_{3'',6''}$), 7.311 (s, 1H, H_4), 7.223 (t, 1H, $^3J_1$= 8.4 Hz, $^3J_2$= 8.0 Hz, $H_{4''}$). ^{13}C NMR (100 MHz, DMSO-d_6) δ/ppm: 165.48 ($C_{quat.}$, C_6), 155.13 ($C_{quat.}$, $C_{2''}$), 154.79 ($C_{quat.}$, C_{5a}), 149.29 (CH, $C_{6''}$), 147.91 ($C_{quat.}$, $C_{4'}$), 147.50 ($C_{quat.}$, C_8), 139.90 ($C_{quat.}$,$C_{5'''}$), 139.10 ($C_{quat.}$, $C_{1'}$), 137.20 (CH, $C_{4''}$), 136.67 ($C_{quat.}$, C_3), 131.90 (CH, $C_{4'''}$), 128.60 (CH, $C_{2'''}$), 128.00 (CH, $C_{3'''}$), 126.20 (CH, $C_{2',6'}$), 123.60 (CH, $C_{5''}$), 124.40 (CH, $C_{3',5'}$), 121.37 (CH, $C_{3''}$), 105.26 (CH, C_7), 93.37 (CH, C_4). [Total signal observed = 19: signal of C and CH_2 = 8 (Ar-C = 2, pyridine-C = 1, thiophene-C = 1, pyrazolo[1,5-a]pyrimidine-C = 4), signal of CH and CH_3 = 11 (Ar-CH = 2, pyridine-CH = 4, thiophene-CH = 3, pyrazolo[1,5-a]pyrimidine-CH = 2)]. FT-IR: (KBr pellet) ν_{max} (cm^{-1}): 3116 $\nu_{(=C-H)ar}$ (w), 1704 $\nu_{(C=N)}$ (s), (w), 1087 $\nu_{(C-S-C)stre.\ (thiophene\ ring)}$ (w), 717 – 840 $\nu_{(ArH)2\ 1612\ \nu(C=C)conjugated\ alkenes}$ (s), 1519 $\nu_{(C-H)banding}$ (s), 1357 $\nu_{(N-O)nitro}$ (w), 1226 $\nu_{(C-C)alkanes}$ (s), 1142 $\nu_{(Ar-NO2)\ adjacent\ hydrogen}$ (m), 585 $\nu_{(=CH)oop\ band}$ (s). Mass (m/z): 400 $[M]^+$.

2.4.5 | 5-(Pyridin-2-yl)-2-(thiophen-2-yl)-7-(tolyl)pyrazolo[1,5-a] pyrimidine (5e)

It was synthesized using chalcone (*E*)-1-(pyridin-2-yl)-3-(p-tolyl)prop-2-en-1-one **(3e)** (0.288 g, 2.8 mmol) and 3-

(thiophene-2-yl)-1*H*-pyrazol-5-amine **(4a)** (0.50 g, 3.0 mmol) as described in general process. Colour: yellow powder, Yield: 81 %, mol. wt. 368.46 gm/mol, m.p. 222 °C; Anal. Calc. (%) For $C_{22}H_{16}N_4S$: C, 71.72; H, 4.38; N, 15.21; S, 8.70. Found (%): C, 72.66; H, 3.89; N, 15.47; S, 8.23. UV-vis: λ (nm) (ε, M^{-1} cm^{-1}): 294.50 (15,830), 358 (3,270). ^{1}H NMR (400 MHz, DMSO-d_6) δ/ppm: 8.779 (d, 1H, J= 8.0 Hz, $H_{2'''}$), 8.766 (d, 1H, J= 8.0 Hz, $H_{4'''}$), 8.311 (d, 2H, J= 8.0 Hz, $H_{2',6'}$), 8.151 (s, 1H, H_7), 8.078 (t, 1H, $^3J_1$= 8.4 Hz, $^3J_2$= 7.6 Hz, $H_{3'''}$), 7.769 (d, 1H, J= 8.0 Hz, $H_{5'}$), 7.658 (d, 1H, J= 7.6 Hz, $H_{3'}$), 7.561 (t, 1H, $^3J_1$= 9.2 Hz, $^3J_2$= 8.8 Hz, $H_{5''}$), 7.369 (s, 1H, H_4), 7.361 - 7.196 (multiplet, 3H, $H_{3'',4'',5''}$), 3.916 (s, 3H, $-CH_3$). ^{13}C NMR (100 MHz, DMSO-d_6) δ/ppm: 165.18 ($C_{quat.}$, C_6), 155.30 ($C_{quat.}$, $C_{2''}$), 154.70 ($C_{quat.}$, C_{5a}), 149.79 (CH, $C_{6''}$), 147.50 ($C_{quat.}$, C_8) 131.70 ($C_{quat.}$, $C_{4'}$), 139.90 ($C_{quat.}$, $C_{5'''}$), 137.20 (CH, $C_{4''}$), 136.67 ($C_{quat.}$, C_3), 131.90 (CH, $C_{4'''}$), 130.00 ($C_{quat.}$, $C_{1'}$), 129.50 (CH, $C_{3',5'}$), 128.60 (CH, $C_{2'''}$), 128.00 (CH, $C_{3'''}$), 125.70 (CH, $C_{2',6'}$), 123.60 (CH, $C_{5''}$), 121.37 (CH, $C_{3''}$), 105.26 (CH, C_7), 93.37 (CH, C_4), 21.50 ($-CH_3$). [Total signal observed = 20: signal of C and CH_2 = 8 (Ar-C = 2, pyridine-C = 1, thiophene-C = 1, pyrazolo[1,5-a]pyrimidine-C = 4), signal of CH and CH_3 = 12 (Ar-CH = 2, pyridine-CH = 4, thiophene-CH = 3, pyrazolo[1,5-a]pyrimidine-CH = 2, -CH3 = 1)]. FT-IR: (KBr pellet) ν_{max} (cm^{-1}): 3108 $\nu_{(=C-H)ar}$ (w), 1708 $\nu_{(C=N)}$ (s), 1614 $\nu_{(C=C)conjugated\ alkenes}$ (s), 1520 $\nu_{(C-H)banding}$ (s), 1226 $\nu_{(C-C)alkanes}$ (s), 1087 $\nu_{(C-S-C)stre.\ (thiophene\ ring)}$ (w),709 – 840 $\nu_{(Ar-H)2\ adjacent\ hydrogen}$ (m), 586 $\nu_{(=C-H)oop\ band}$ (s). Mass (m/z): 369 $[M]^+$.

2.4.6 | 7-Phenyl-5-(pyridin-2-yl)-2-(thiophen-2yl)pyrazolo[1,5-a] pyrimidine (5f)

It was synthesized using chalcone (*E*)-3-phenyl-1-(pyridin-2-yl)prop-2-en-1-one **(3f)** (0.246 g, 2.8 mmol) and 3-(thiophene-2-yl)-1*H*-pyrazol-5-amine **(4a)** (0.50 g, 3.0 mmol) as described in general process. Colour: yellow powder, Yield: 78 %, mol. wt. 354.43 gm/mol, m.p. 228 °C; Anal. Calc. (%) For $C_{21}H_{14}N_4S$: C, 71.17; H, 3.98; N, 15.81; S, 9.05. Found (%): C, 71.89; H, 3.23; N, 15.96; S, 8.90. UV-vis: λ (nm) (ε, M^{-1} cm^{-1}): 294 (35,840), 357 (9,270). ^{1}H NMR (400 MHz, DMSO-d_6) δ/ppm: 8.783 (t, 1H, $^3J_1$= 4.4 Hz, $^3J_2$= 4.4 Hz, $H_{3'''}$), 8.499 (dd, 2H, $^3J_1$= 8.0 Hz, ^{4} J_2= 10.8 Hz, $H_{4'''}$), 8.28-8.205 (multiplet, 1H, $H_{2'''}$), 8.161 (d, 1H, J= 10.4 $H_{4''}$), 8.126 (s, 1H, H_7), 8.066 (t, 1H, $^3J_1$= 6.8 Hz, $^3J_2$= 6.4 HZ, $H_{5''}$), 7.663 (d, 2H, J= 5.2 Hz, $H_{2',6'}$), 7.495 (d, 1H, J= 5.6 Hz, $H_{4'''}$), 7.587 (dd, 2H, $^3J_1$= 8.4 Hz, ^{4} J_2= 4.4 Hz, $H_{3',5'}$), 7.360 (s, 1H, H_4), 7.213 (t, 1H, $^3J_1$= 4.4 Hz, $^3J_2$= 5.2 Hz, $H_{4'}$). ^{13}C NMR (100 MHz, DMSO-d_6) δ/ppm: 165.18 ($C_{quat.}$, C_6), 155.3 ($C_{quat.}$, $C_{2''}$), 154.70 ($C_{quat.}$, C_{5a}), 149.79 (CH, $C_{6''}$), 147.5 ($C_{quat.}$, C_8) 131.9 (CH, $C_{4'''}$), 140.0 ($C_{quat.}$, $C_{1'}$), 139.9 ($C_{quat.}$, $C_{5'''}$), 137.2 (CH, $C_{4''}$), 136.67 ($C_{quat.}$, C_3), 129.5 (CH, $C_{3',5'}$), 128.7 (CH, $C_{4'}$), 128.6 (CH, $C_{2'''}$), 128.0 (CH, $C_{3'''}$), 127.5 (CH, $C_{2',6'}$), 123.37 (CH, $C_{5''}$), 121.4 (CH, $C_{3''}$), 105.26 (CH, C_7), 93.37 (CH, C_4). [Total signal observed = 19: signal of C and CH_2 = 7 (Ar-C = 1, pyridine-C = 1, thiophene-C = 1, pyrazolo[1,5-a]pyrimidine-C = 4), signal of CH and CH_3 = 12 (Ar-CH = 3, thiophene-CH = 3, pyrazolo[1,5-a]pyrimidine-CH = 2, pyridine-CH = 4)]. FT-IR: (KBr pellet) ν_{max} (cm^{-1}): 3117 $\nu_{(=C-H)ar}$ (w), 1717 $\nu_{(C=N)}$ (s), 1612 $\nu_{(C=C)conjugated\ alkanes}$ (s), 1473 - 1566 $\nu_{(C-H)banding}$ (s), 1220 $\nu_{(C-C)alkanes}$ (s), 1056 $\nu_{(C-S-C)stre.\ (thiophene\ ring)}$ (m) 717 - 817 $\nu_{(Ar-H)2\ adjacent\ hydrogen}$ (s), 586 $\nu_{(=C-H)\ oop\ band}$ (s). Mass (m/z): 355 $[M]^+$.

2.5 | General synthesis of binuclear Pt^{II} complexes (6a - 6f)

The pyrazolo[1,5-a]pyrimidine derived ligands coordinate with Pt^{II} metal ion forming complexes were prepared following published method.[20,21] The 2 ml aqueous solution of K_2PtCl_4 (0.2 mmol) was mixed with a solution of ligands, (5a-5f) (0.1 mmol) respectively 2:1 molar ratio in methanol (20 ml) and then refluxed for 5-6 h. After cooling, the resulting reddish brown slurry was filtered and the complexes obtained in high yields after filtration and evaporation of solvents. The products were collected after washing with methanol twice. The proposed reaction for the synthesis of complexes (6a-6f) is shown in Scheme 1. ^{1}H NMR, ^{13}C NMR spectra of complexes (6a-6b) are shown in supplementary material 1 and 2, respectively.

2.6 | Synthesis of $[Pt_2(5a)(Cl_4)]$ (6a)

It was synthesized using ligand (5a) (0.036 g, 0.1 mmol) and K_2PtCl_4 salt (0.083 g, 0.2 mmol) as described in general process. Colour: brown powder, Yield: 88 %, mol. wt. 916.43 g/mol, m.p. ≥ 300 °C; Anal. Calc. (%) For $C_{22}H_{16}Cl_4N_4OPt_2S$: C, 27.03; H, 1.45; N, 6.11; S, 5.50; Pt, 42.08. Found (%): C, 27.39; H, 1.10; N, 5.78; S, 5.11; Pt, 41.95. Conductance: 25 Ω^{-1} cm^2 mol^{-1}. UV-vis: λ (nm) (ε, M^{-1} cm^{-1}): 307 (37,110), 358 (11,620), 472 (1,620). ^{1}H NMR (400 MHz, DMSO-d_6) δ/ppm: 9.591 (d, 1H, J= 7.6 Hz, $H_{2'''}$), 8.973 (d, 1H, J= 7.6 Hz, $H_{4'''}$), 8.589 (s, 1H, H_7), 8.479 (t, 1H, $^3J_1$= 8.0 Hz, ^{3} J_2= 8.0 Hz, $H_{3'''}$), 8.336 (d, 1H, J= 7.6 Hz, $H_{5'}$), 8.283 (s, 1H, H_4), 7.878 (t, 1H, $^3J_1$= 7.6 Hz, ^{3} J_2= 8.0 Hz, $H_{5''}$), 7.763 (dd, 2H, $^3J_1$= 8.0 Hz, ^{4} J_2= 4.0 Hz, $H_{3'',6''}$), 7.651 (d, 1H, J= 7.6 Hz, $H_{3'}$), 7.259 – 7.295 (multiplet, 3H, $H_{4'',2',6'}$), 3.948 (s, 3H, $-OCH_3$). ^{13}C NMR (100 MHz, DMSO-d_6) δ/ppm: 160.64 ($C_{quat.}$, $C_{4'}$), 150.99 ($C_{quat.}$, C_8), 150.15 ($C_{quat.}$, $C_{2''}$), 144.05 ($C_{quat.}$, C_{5a}), 142.87 (CH, $C_{6''}$), 142.30 (CH, $C_{4''}$), 139.38

(CH, $C_{3'''}$), 137.21 ($C_{quat.}$, C_6), 134.48 (CH, $C_{4'''}$), 128.85 (CH, $C_{2',6'}$), 125.33 ($C_{quat.}$, $C_{1'}$), 125.10 (CH, $C_{5''}$), 122.09 (CH, $C_{3''}$), 121.63 (CH, C_4), 121.22 (CH, C_7), 116.00 (CH, $C_{2'''}$), 114.81 (CH, $C_{3',5'}$), 114.62 ($C_{quat.}$, $C_{5'''}$), 107.06 ($C_{quat.}$, C_3), 55.82 (O-CH_3). [Total signal observed = 20: signal of C and CH_2 = 8 (Ar-C = 2, pyridine-C = 1, thiophene-C = 1, pyrazolo[1,5-a]pyrimidine-C = 4), signal of CH and CH_3 = 12 (Ar-CH = 2, thiophene-CH = 3, pyrazolo[1,5-a]pyrimidine-CH = 2, pyridine-CH = 4, -OCH_3 = 1)]. FT-IR: (KBr pellet) ν_{max} (cm^{-1}): 3078 $\nu_{(=C-H)ar}$ (w), 1596 $\nu_{(C=N)}$ (s), 1566 $\nu_{(C=C)conjugated\ alkenes}$ (s), 1512 – 1473 $\nu_{(C-H)banding}$ (s), 1249 $\nu_{(C-C)alkanes}$ (s), 1180 $\nu_{(Ar-O-CH3)}$ (s), 1021 $\nu_{(C-S-C)stre.\ (thiophene\ ring)}$ (s), 717 – 840 $\nu_{(Ar-H)2\ adjacent\ hydrogen}$ (s), 640 $\nu_{(N-Pt)}$ (s), 555 $\nu_{(S-Pt)}$ (s).

2.7 | Synthesis of [Pt_2(5b)(Cl_4)] (6b)

It was synthesized using ligand **(5b)** (0.037 g, 0.1 mmol) and K_2PtCl_4 salt (0.083 g, 0.2 mmol) as described in general process. Colour: brown powder, Yield: 85 %, mol. wt. 904.39 g/mol, m.p. ≥ 300 °C; Chemical formula: $C_{21}H_{13}Cl_4FN_4Pt_2S$. Conductance: 19 $\Omega^{-1}cm^2\ mol^{-1}$. UV-vis: λ (nm) (ε, $M^{-1}\ cm^{-1}$): 304 (38,020), 357 (10,920), 471.50 (1,820). ^{1}H NMR (400 MHz, DMSO-d_6) δ/ppm: 9.654 (d, 1H, J= 8.0 Hz, $H_{2'''}$), 8.964 (d, 1H, J= 8.0 Hz, $H_{4'''}$), 8.694 (s, 1H, H_7), 8.524 - 8.418 (multiplet, 3H, $H_{3',5',5''}$), 8.298 (s, 1H, H_4), 7.937 (t, 1H, $^3J_1$= 7.6 Hz, $^3J_2$= 8.0 Hz, $H_{3'''}$), 7.774 (d, 1H, J= 8.0 Hz, $H_{2',6'}$), 7.702 (d, 1H, J= 8.0 Hz, $H_{6'}$), 7.633 (dd, 2H, $^3J_1$= 8.0 Hz, $^4J_2$= 4.8 Hz, $H_{3'',6''}$), 7.249 (t, 1H, $^3J_1$= 8.0 Hz, $^3J_2$= 8.0 Hz, $H_{4''}$). ^{13}C NMR (100 MHz, DMSO-d_6) δ/ppm: 162.91 ($C_{quat.}$, $C_{4'}$), 150.95 ($C_{quat.}$, C_8), 150.18 ($C_{quat.}$, $C_{2''}$), 144.15 ($C_{quat.}$, C_{5a}), 142.89 (CH, $C_{6''}$), 142.20 (CH, $C_{4''}$), 139.31 (CH, $C_{3'''}$), 137.26 ($C_{quat.}$, C_6), 134.43 (CH, $C_{4'''}$), 130.56 (CH, $C_{2',6'}$), 128.37 ($C_{quat.}$, $C_{1'}$), 125.18 (CH, $C_{5''}$), 122.19 (CH, $C_{3''}$), 121.69 (CH, C_4), 121.20 (CH, C_7), 116.30 (CH, $C_{2'''}$), 116.71 (CH, $C_{3',5'}$), 114.68 ($C_{quat.}$, $C_{5'''}$), 107.09 ($C_{quat.}$, C_3). [Total signal observed = 19: signal of C and CH_2 = 8 (Ar-C = 2, thiophene-C = 1, pyrazolo[1,5-a]pyrimidine-C = 4, pyridine –C = 1), signal of CH and CH_3 = 11 (Ar-CH = 2, thiophene-CH = 3, pyrazolo[1,5-a]pyrimidine-CH = 2, pyridine-CH = 4)]. FT-IR: (KBr pellet) ν_{max} (cm^{-1}): 3078 $\nu_{(=C-H)ar}$ (m), 1604 – 1566 $\nu_{(C=N)}$ (s), 1512 – 1481 $\nu_{(C=C)conjugated\ alkenes}$ (s), 1411 $\nu_{(C-H)banding}$ (m), 1226 $\nu_{(C-C)alkanes}$ (s), 1157 $\nu_{(Ar-F)}$ (s), 1018 $\nu_{(C-S-C)stre.\ (thiophene\ ring)}$ (w), 725 – 840 $\nu_{(Ar-H)2\ adjacent\ hydrogen}$ (s), 632 $\nu_{(N-Pt)}$ (s), 570 $\nu_{(S-Pt)}$ (s).

2.8 | Synthesis of [Pt_2(5c)(Cl_4)] (6c)

It was synthesized using ligand **(5c)** (0.038 g, 0.1 mmol) and K_2PtCl_4 salt (0.083 g, 0.2 mmol) as described in general process. Colour: brown powder, Yield: 88 %, mol. wt. 920.84 g/mol, m.p. ≥ 300 °C; Anal. Calc. (%) For $C_{21}H_{13}Cl_5FN_4Pt_2S$: C, 27.69; H, 1.42; N, 6.08; S, 3.48; Pt, 42.37. Found (%): C, 28.19; H, 1.49; N, 6.57; S, 3.21; Pt, 42.18. Conductance: 21 $\Omega^{-1}\ cm^2\ mol^{-1}$. UV-vis: λ (nm) (ε, $M^{-1}\ cm^{-1}$): 308 (35,420), 358 (9,820), 472.50 (1,580). ^{1}H NMR (400 MHz, DMSO-d_6) δ/ppm: 9.670 (d, 1H, J= 7.2 Hz, $H_{2'''}$), 8.951 (d, 1H, J= 7.6 Hz, $H_{4'''}$), 8.502 (dd, 2H, $^3J_1$= 8.0 Hz, $^4J_2$= 4.0 Hz, $H_{3'',6''}$), 8.370 (d, 1H, J= 8.8 Hz, $H_{5'}$), 8.304 (s, 1H, H_7), 7.896 (t, 1H, $^3J_1$= 7.6 Hz, $^3J_2$= 7.6 Hz, $H_{3'''}$), 7.832 – 7.744 (multiplet, 4H, $H_{3',2',6',5''}$), 7.669 (s, 1H, H_4), 7.228 (t, 1H, $^3J_1$= 8.8 Hz, $^3J_2$= 8.8 Hz, $H_{4''}$). ^{13}C NMR (100 MHz, DMSO-d_6) δ/ppm: 150.91 ($C_{quat.}$, C_8), 150.18 ($C_{quat.}$, $C_{2''}$), 144.15 ($C_{quat.}$, C_{5a}), 142.89 (CH, $C_{6''}$), 142.20 (CH, $C_{4''}$), 139.31 (CH, $C_{3'''}$), 137.26 ($C_{quat.}$, C_6), 134.83 (CH, $C_{4'''}$), 134.3($C_{quat.}$, $C_{4'}$), 128.56 (CH, $C_{2',6'}$), 131.1 ($C_{quat.}$, $C_{1'}$), 125.18 (CH, $C_{5''}$), 122.89 (CH, $C_{3''}$), 121.67 (CH, C_4), 121.20 (CH, C_7), 116.00 (CH, $C_{2'''}$), 129.3 (CH, $C_{3',5'}$), 114.68 ($C_{quat.}$, $C_{5'''}$), 107.39 ($C_{quat.}$, C_3). [Total signal observed = 19: signal of C and CH_2 = 8 (Ar-C = 2, thiophene-C = 1, pyrazolo[1,5-a]pyrimidine-C = 4, pyridine –C = 1), signal of CH and CH_3 = 11 (Ar-CH = 2, thiophene-CH = 3, pyrazolo[1,5-a]pyrimidine-CH = 2, pyridine-CH = 4)]. FT-IR: (KBr pellet) ν_{max} (cm^{-1}): 3085 $\nu_{(=C-H)ar}$ (w), 1596 – 1566 $\nu_{(C=N)}$ (m), 1519 – 1473 $\nu_{(C=C)conjugated\ alkenes}$ (s), 1396 $\nu_{(C-H)banding}$ (m), 1226 $\nu_{(C-C)alkanes}$ (s), 1149 $\nu_{(Ar-Cl)}$ (w), 1010 $\nu_{(C-S-C)stre.\ (thiophene\ ring)}$ (s), 817 – 717 $\nu_{(Ar\ -H)2\ adjacent\ hydrogen}$ (s), 624 $\nu_{(N-Pt)}$ (s), 555 $\nu_{(S-Pt)}$ (s).

2.9 | Synthesis of [Pt_2(5d)(Cl_4)] (6d)

It was synthesized using ligand **(5d)** (0.039 g, 0.1 mmol) and K_2PtCl_4 salt (0.083 g, 0.2 mmol) as described in general process. Colour: brown powder, Yield: 90 %, mol. wt. 931.40 g/mol, m.p. ≥ 300 °C; Anal. Calc. (%) For $C_{21}H_{13}Cl_4N_5O_2Pt_2S$: C, 27.08; H, 1.41; N, 7.52; S, 3.44; Pt, 41.89. Found (%): C, 26.58; H, 1.5; N, 6.83; S, 3.10; Pt, 42.04. Conductance: 22 $\Omega^{-1}\ cm^2\ mol^{-1}$. UV-vis: λ (nm) (ε, $M^{-1}\ cm^{-1}$): 305 (34,820), 357 (8,790), 470.50 (1,680). ^{1}H NMR (400 MHz, DMSO-d_6) δ/ppm: 8.575 (d, 2H, J= 8.0 Hz, $H_{2''',4'''}$), 8.520 (d, 2H, J= 8.4 Hz, $H_{3',5'}$), 8.199 (s, 1H, H_7), 8.115 (d, 1H, J= 8.8 Hz, $H_{2'}$), 7.935 (d, 1H, J= 7.2 Hz, $H_{6'}$), 7.789 (dd, 2H, $^3J_1$= 8.8 Hz, $^4J_2$= 3.2 Hz, $H_{3'',6''}$), 7.717 – 7.662 (multiplet, 1H, $H_{5''}$), 7.619 (t, 1H, $^3J_1$= 7.6 Hz, $^3J_2$= 8.0 Hz, $H_{3''}$), 7.399 (s, 1H, H_4), 7.242 (t, 1H, $^3J_1$= 7.2 Hz, $^3J_2$= 7.6 Hz, $H_{4''}$). ^{13}C NMR (100 MHz, DMSO-d_6) δ/ppm: 150.88 ($C_{quat.}$, C_8), 150.18 ($C_{quat.}$, $C_{2''}$), 147.37 ($C_{quat.}$, $C_{4'}$), 144.15 ($C_{quat.}$, C_{5a}), 142.89 (CH, $C_{6''}$), 142.20 (CH, $C_{4''}$), 139.81 (CH, $C_{2'''}$), 139.26 ($C_{quat.}$, $C_{1'}$), 137.1 ($C_{quat.}$, C_6), 134.83 (CH, $C_{4'''}$), 126.25 (CH, $C_{2',6'}$), 125.18 (CH, $C_{5''}$), 122.89 (CH, $C_{3''}$), 121.77 (CH, C_4), 121.20 (CH, C_7), 116.00 (CH, $C_{2'''}$), 124.4 (CH, $C_{3',5'}$), 114.68 ($C_{quat.}$, $C_{5'''}$), 107.39 ($C_{quat.}$, C_3).

[Total signal observed = 19: signal of C and CH_2 = 8 (Ar-C = 2, thiophene-C = 1, pyrazolo[1,5-a]pyrimidine-C = 4, pyridine –C = 1), signal of CH and CH_3 = 11 (Ar-CH = 2, thiophene-CH = 3, pyrazolo[1,5-a]pyrimidine-CH = 2, pyridine-CH = 4)]. FT-IR: (KBr pellet) ν_{max} (cm^{-1}): 3078 $\nu_{(=C-H)ar}$ (w), 1596 – 1566 $\nu_{(C=N)}$ (s), 1519 – 1473 $\nu_{(C=C)conjugated\ alkenes}$ (s), 1342 $\nu_{(C-H)banding}$ (s), 1226 $\nu_{(C-C)alkanes}$ (s), 1149 $\nu_{(Ar-NO2)}$ (w), 1010 $\nu_{(C-S-C)stre\ (thiophene\ ring)}$ (w), 848 – 717 $\nu_{(Ar-H)2\ adjacent\ hydrogen}$ (s), 632 $\nu_{(N-Pt)}$ (s), 555 $\nu_{(S-Pt)}$ (s).

2.10 | Synthesis of $[Pt_2(5e)(Cl_4)]$ (6e)

It was synthesized using ligand **(5e)** (0.0367 g, 0.1 mmol) and K_2PtCl_4 salt (0.083 g, 0.2 mmol) as described in general process. Colour: brown powder, Yield: 82 %, mol. wt. 900.43 g/mol, m.p. ≥ 300 °C; Anal. Calc. (%) For $C_{22}H_{16}Cl_4N_4Pt_2S$: C, 29.35; H, 1.89; N, 6.92; S, 3.56; Pt, 43.33. Found (%): C, 28.58; H, 2.1; N, 7.09; S, 3.07; Pt, 43.04. Conductance: 18 Ω^{-1} cm^2 mol^{-1}. UV-vis: λ (nm) (ε, M^{-1} cm^{-1}): 307 (36,200), 359 (9,790), 471 (1,790). ^{1}H NMR (400 MHz, DMSO-d_6) δ/ppm: 8.799 (d, 1H, J= 8.0 Hz, $H_{2'''}$), 8.678 (s, 1H, H_7), 8.535 (d, 1H, J= 8.0 Hz, $H_{4'''}$), 8.278 (t, 1H, $^3J_1$= 8.4 Hz, $^3J_2$= 8.4 Hz, $H_{3'''}$), 8.175 – 8.059 (multiplet, 2H, $H_{3',5'}$), 7.756 (d, 1H, J= 7.2 Hz, $H_{2'}$), 7.654 (d, 1H, J= 7.2 Hz, $H_{6'}$), 7.604 (t, 1H, $^3J_1$= 7.2 Hz, $^3J_2$= 7.2 Hz, $H_{5''}$), 7.513 (dd, 2H, $^3J_1$= 8.0 Hz, ^{4} J_2= 4.0 Hz, $H_{3'',6''}$), 7.317 (s, 1H, H_4), 7.227 (t, 1H, $^3J_1$= 7.6 Hz, ^{3} J_2= 7.6 Hz, $H_{4''}$), 4.173 (s, 3H, -CH_3). ^{13}C NMR (100 MHz, DMSO-d_6) δ/ppm: 150.98 ($C_{quat.}$, C_8), 150.18 ($C_{quat.}$, $C_{2''}$), 131.72 ($C_{quat.}$, $C_{4'}$), 144.50 ($C_{quat.}$, C_{5a}), 142.89 (CH, $C_{4''}$), 142.20 (CH, $C_{6''}$), 139.81 (CH, $C_{3'''}$), 137.26 ($C_{quat.}$, C_6), 134.16 (CH, $C_{4'''}$), 130.83 ($C_{quat.}$, $C_{1'}$), 129.66 (CH, $C_{3',5'}$), 125.78 (CH, $C_{2',6'}$), 125.39 (CH, $C_{5''}$), 122.77 (CH, $C_{3''}$), 121.70 (CH, C_4), 121.22 (CH, C_7), 116.00 (CH, $C_{2'''}$), 114.68 ($C_{quat.}$, $C_{5'''}$), 107.39 ($C_{quat.}$, C_3). 21.56 (-CH_3). [Total signal observed = 20: signal of C and CH_2 = 8 (Ar-C = 2, thiophene-C = 1, pyrazolo[1,5-a]pyrimidine-C = 4, pyridine –C = 1), signal of CH and CH_3 = 12 (Ar-CH = 2, thiophene-CH = 3, pyrazolo[1,5-a]pyrimidine-CH = 2, pyridine-CH = 4, -CH_3 = 1)]. FT-IR: (KBr pellet) ν_{max} (cm^{-1}): 3078 $\nu_{(=C-H)ar}$ (w), 1596 -1566 $\nu_{(C=N)}$ (s), 1512 -1473 $\nu_{(C=C)conjugated\ alkenes}$ (m), 1396 $\nu_{(C-H)banding}$ (m), 1218 $\nu_{(C-C)alkanes}$ (s), 1026 $\nu_{(C-S-C)stre.\ (thiophene\ ring)}$, (w), 794 – 717 $\nu_{(Ar-H)2\ adjacent\ hydrogen}$ (s), 601 $\nu_{(N-Pt)}$ (s), 532 $\nu_{(S-Pt)}$ (s).

2.11 | Synthesis of $[Pt_2(5f)(Cl_4)]$ (6f)

It was synthesized using ligand **(5f)** (0.035 g, 0.1 mmol) and K_2PtCl_4 salt (0.083 g, 0.2 mmol) as described in general process. Colour: brown powder, Yield: 80 %, mol. wt. 886.40 g/mol, m.p. ≥ 300 °C; Anal. Calc. (%) For $C_{21}H_{14}Cl_4N_4Pt_2S$: C, 28.76; H, 1.59; N, 6.32; S, 3.62; Pt, 44.02. Found (%): C, 29.03; H, 1.81; N, 6.01; S, 3.34; Pt, 44.24. Conductance: 20 Ω^{-1} cm^2 mol^{-1}. UV-vis: λ (nm) (ε, M^{-1} cm^{-1}): 306 (37,820), 357 (11,500), 472.50 (1,570). ^{1}H NMR (400 MHz, DMSO-d6) δ/ppm: 8.894 (t, 1H, $^3J_1$= 8.0 Hz, ^{3} J_2= 8.0 Hz, $H_{3'''}$), 8.583 (dd, 2H, $^3J_1$= 8.8 Hz, $^4J_2$= 4.0 Hz, $H_{3'',6''}$), 8.334 – 8.233 (multiplet, 3H, $H_{2''',4''',5''}$), 8.110 (s, 1H, H_7), 7.879 – 7.610 (multiplet, 5H, $H_{2',3',4',5',6'}$), 7.329 (s, 1H, H_4), 7.282 (t, 1H, $^3J_1$= 8.0 Hz, ^{3} J_2= 8.0 Hz, $H_{4''}$). ^{13}C NMR (100 MHz, DMSO-d_6) δ/ppm: 150.98 ($C_{quat.}$, C_8), 150.18 ($C_{quat.}$, $C_{2''}$), 144.50 ($C_{quat.}$, C_{5a}), 142.89 (CH, $C_{6''}$), 142.20 (CH, $C_{4''}$), 139.81 (CH, $C_{3'''}$), 137.26 ($C_{quat.}$, C_6), 134.16 (CH, $C_{4'''}$), 133.03 ($C_{quat.}$, $C_{1'}$), 130.05 (CH, $C_{3',5'}$), 127.78 (CH, $C_{2',6'}$), 128.39 (CH, $C_{4'}$), 125.77 (CH, $C_{5''}$), 122.9(CH, $C_{3''}$), 121.72 (CH, C_7), 121.19 (CH, C_4), 116.00 (CH, $C_{2'''}$), 114.68 ($C_{quat.}$, $C_{5'''}$), 107.49 ($C_{quat.}$, C_3). [Total signal observed = 19: signal of C and CH_2 = 8 (Ar-C = 2, thiophene-C = 1, pyrazolo[1,5-a]pyrimidine-C = 4, pyridine –C = 1), signal of CH and CH_3 = 11 (Ar-CH = 2, thiophene-CH = 3, pyrazolo[1,5-a]pyrimidine-CH = 2, pyridine-CH = 4)]. FT-IR: (KBr pellet) ν_{max} (cm^{-1}): 3078 $\nu_{(=C-H)ar}$ (w), 1558 – 1596 $\nu_{(C=N)}$ (s), 1519 – 1473 $\nu_{(C=C)conjugated\ alkenes}$ (m), 1350 $\nu_{(C-H)banding}$ (s), 1226 $\nu_{(C-C)alkanes}$ (s), 1033 $\nu_{(C-S-C)stre.\ (thiophene\ ring)}$ (w), 848 – 702 $\nu_{(Ar-H)2\ adjacent\ hydrogen}$ (s), 648 $\nu_{(N-Pt)}$ (s), 555 $\nu_{(S-Pt)}$ (s).

2.12 | Biological screening of synthesized binuclear Pt^{II} complexes

2.12.1 | *In vitro* antibacterial activity

To examine antibacterial activity of compounds under investigation, we used five test organisms such as two $Gram^{(+ve)}$ *Bacillus subtilis* and *Staphylococcus aureus* and three $Gram^{(-ve)}$ *Escherichia coli*, *Pseudomonas aeruginosa* and *Serratia marcescens* using the broth dilution technique. A pre-culture of bacteria was used to prepare bacterial culture in Luria Broth. DMSO was used as medium to acquire preferred concentration of compounds to check upon microbial strains. The test compounds of specific concentration was added to the sugar tube containing Luria Broth solution and sterilized in autoclave before the addition of previously cultured bacterial species. After adding different bacterial species to the tubes containing specific concentration of test compounds, it was allowed to incubate for 24 h at optimum temperature. Experiment was repeated till only a faint turbidity appears in the tube. The lowest concentration, which showed no visible growth after 24 h subculture was considered as MIC for each compound.[22,23]

2.13 | Cellular level bioassay using *S. Pombe* cells

Cellular level bioassay was carried out using *Schizosaccharomyces Pombe* cells, which were grown in

liquid yeast extract media in a 150 ml Erlenmeyer flask containing 50 ml of yeast extract media. The flask was incubated at 30 °C on a shaker at 160 rpm until the exponential growth of *S. Pombe* was obtained after 24 to 30 h. Then, the cell culture was treated with the different concentrations (20, 40, 60, 80, 100 μM) of the synthesized complexes, free ligands, K_2PtCl_4 salt and also with dimethyl sulphoxide as a control and after further allowed to grow for 16-18 h. Than the next day, by centrifugation at 10, 000 rpm for 10 min, the treated cells were collected and dissolved in 500 μL of PBS (Phosphate Buffered Saline) 80 μL of yeast culture dissolved in PBS and 20 μL of 0.4% trypan blue prepared in PBS were mixed and cells were observed with a compound microscope (40X). The dye could enter dead cells only so they appeared blue, whereas live cells resisted the entry of dye. The number of dead cells and number of live cells were counted in one field. Cell counting was repeated in two more fields and the average percentage of dead cells due to the synthesized compounds were calculated.[24]

2.14 | *In vitro* cytotoxic study using brine shrimp lethality bioassay (BSLB)

Cytotoxicity assays are widely used by the pharmaceutical industry to screen for cytotoxicity in compound libraries. Researchers can look for cytotoxic compounds, if they are interested in developing a therapeutic that targets rapidly dividing cancer cells. *In vitro* cytotoxicity is a method by which one can check the toxicity of the compounds on Brine Shrimp. The experiment was carried out following the protocol of Mayer *et al*. A set of 2, 4, 8, 16, 20 μg/ml in test tube was prepared from a stock solution of 1000 μg/ml of the test compounds. Final volume of in each test tube was adjusted to 2500 μL (1000 μL sea salt solution, 450 μL double distilled water, 50 μL DMSO + complex and remaining 1000 μL was added as 10 nauplii in a sea salt solution). After 24 h numbers of dead nauplii were counted and from the survival LC_{50} was calculated.[25]

2.15 | *Mycobacterium tuberculosis* (Mtb) H_{37}Rv strain

A primary *in vitro* antituberculosis activity of the synthesized binuclear Pt^{II} complexes were conducted at concentration of 250 μg/ml against Mycobacterium tuberculosis H_{37}Rv strain by using Lowenstein - Jensen medium as described by Rattan [26]. The obtained results of synthesized complex are presented in result and discussion.

2.16 | *In vitro* antiproliferative cytotoxicity on human colorectal carcinoma HCT-116 cells

Antiproliferative cytotoxicity of the synthesized Pt^{II} complexes (6a-6f) was determined by means of the MTT (3-(4,5-dimethyl-2-thiazolyl)-2,5-diphenyl-2H-tetrazolium bromide) assay. The HCT-116 cells were plated at 5000 cells per well in 96-well culture plates with a culture medium, incubated for 24 h at 37 °C in a 5% CO_2 incubator. The concentrations of compounds exhibit the vehicle control (0.5% DMSO), DMSO, 10, 50, 100, 250, 500, 1000 μg/ml. The cells were washed twice with Dulbecco's Phosphate-Buffered Saline (DPBS) and incubated with 0.5 mg/ml MTT solution for 4 h at 37 °C. Subsequently, 0.1 mL of SDS-HCl was added to each well, mixed carefully and allowed for incubation in the dark for 20 min at 37 °C. Finally, the absorbance of each well was recorded at 570 nm with a reference wavelength of 650 nm using a multimedia micro plate reader (Spectra Max M2e, Molecular devices, Sunnyvale, California, USA). IC_{50} values were calculated from the chart of the cell proliferation (%) against the compound concentration (μg/mL). The results are represented as percentage of cell proliferation in different treatment group. All experiments were carried out in triplicate.[27]

2.17 | DNA interaction studies

2.17.1 | DNA binding study by absorption analysis

The stock solutions of Pt^{II} complexes were prepared using 5% DMSO at 4 °C for complete dissolution and used within 4 days and then diluting them suitably with phosphate buffer (in MilliQ water) to the required concentrations for all the experiments.[4,28] Ratio of UV absorbance kept at 260 and 280 nm was about 1.89:1 for HS-DNA in the buffer, indicating that the HS DNA sufficiently free from protein. The HS-DNA concentration per nucleotide was determined spectrophotometrically by employing an extinction coefficient of 12858 M^{-1} cm^{-1} at 260 nm.

2.18 | Viscosity measurements

The binding of small molecules to DNA cannot be determined only by absorption titration method.[29] Viscometric measurement is a supporting tool to confirm the binding mode. The molecule can bind to DNA by three binding modes as represented below. In electrostatic and groove binding viscosity of DNA solution remain unaltered, while in classical intercalative binding viscosity

will rise. Among these interactions, intercalation and groove binding are the most important DNA-binding modes as they invariably lead to cellular degradation. Herein, we carried out viscosity measurement at 27 ± 0.1 °C using a constant thermometric bath,[30,31]

2.19 | Molecular modeling study with HS DNA

The most stable configuration was chosen as input for investigation and the rigid molecular docking study was performed by using HEX 8.0 software. Pt^{II} complexes were taken from their enhanced structure as a molecule and converted to (Protein Data Bank) .pdb format using CHIMERA 1.5.1 software. HS-DNA used in the experimental work was too large for current computational resources to dock, therefore, the structure of the DNA of sequence d(ACCGACGTCGGT)2 (1BNA) for groove binding and an octamer d(GAAGCTTC)2 (1BNA) for intercalation[32] (PDB id: 1BNA, a familiar sequence used in oligodeoxynucleotide study) obtained from the Protein Data Bank (http://www.rcsb.org/pdb). All calculations were done using on an Intel CORE i5, 2.5 GHz based machine running MS Windows 8 64 bit as the operating system. The by default parameters were used for the docking calculation with correlation type shape only, FFT mode at 3D level, grid dimension of 6 with receptor range 180 and ligand range 180 with twist range 360 and distance range 40.

2.20 | Competitive displacement assay

The competitive interaction of all the complexes was studied by fluorescence quenching analysis in order to find out whether the compound can partially displace ethidium bromide (EB = 3,8-diamino-5-ethyl-6-phenylphenanthridinium bromide) from DNA-EB complex. Ethidium bromide displacement experiment was done by adding the solution of the complexes to the phosphate buffer solution (pH, 7.2) up to the value of r = 3.33 ([DNA]/[Complex]) of pre-treated EB–DNA mixture ([EB] = 33.3 μM, [DNA] = 10 μM). The changes in fluorescence intensities of EB and EB bound to DNA were measured with respect to different concentration of the complex. The EB has less-emission intensity in phosphate buffer solution (pH, 7.2) due to florescence quenching of free EB by the solvent molecules. In the presence of DNA, EB exhibits higher intensity due to its partial intercalative binding mode to DNA. A competitive interaction of the metal complexes to HS DNA results in the displacement of the bound EB and inner filter effect (IFE) were carried out by equation in literature.[33] Therefore, it is needed to eliminate IFE interference with the results. A competitive interaction of the metal complexes to HS DNA results in the displacement of the bound EB.[34] The quenching constant (K_{sq}) was calculated using the linear Stern-Volmer equation (1):[35]

$$\frac{I^0}{I} = Ksq\ r + 1\ OR\ I_0/I = Ksq[Q] + 1 \quad (1)$$

where, I_0 and I are the emission intensity of EB-DNA in the absence and presence of quencher (complex), K_{sq} is the linear Stern-Volmer quenching constant obtained from the plot of I_0/I versus [Q] and r is the ratio of total concentration of complex of DNA or concentration of quencher [Q].

To determine the strength of the interaction of complexes with DNA, the value of the associative binding constant (K_a) was calculated using the Scatchard equation 2:[36]

$$\log I_0{-}I/I = \log Ka + n\log[Q] \quad (2)$$

where, I_0 and I are the fluorescence intensities of the EB-DNA in the absence and presence of different concentrations of complexes, respectively and n is the number of binding. The acting forces between drugs and biomacromolecules include hydrogen bonds, van der Waals forces, electrostatic attraction and hydrophobic interaction, etc. In order to estimate the interaction force of with all compounds, the standard free energy changes (ΔG^0) for the binding process have been calculated using the Van't Hoff equation 3:[37]

$$\Delta G0 = -RTlnKa \quad (3)$$

where, T is the temperature (25 °C, 298 K here), K_a is associative binding constant and R is gas constant 8.314 $Jmol^{-1}\ K^{-1}$. The negative sign for ΔG means that the spontaneous binding process.

2.21 | DNA cleavage assay

The DNA cleavage experiments were performed as follows: A mixture of TAE buffer (0.04 mol L^{-1} Tris–Acetate, pH 8, 0.001 mol L^{-1} edta), 15 μL reaction mixture containing 300 μg/ml plasmid DNA in TE buffer (10 mmol L^{-1} Tris, 1 mmol L^{-1} edta, pH 8.0) and 200 μmol L^{-1} complex solution. Reactions were allowed to proceed for 3 h at 37 °C in the dark and reactions were settled by addition of 5 μL loading buffer a dye solution (0.25% bromophenol blue, 40% sucrose, 0.25% xylene cyanol and 200 mmol L^{-1} edta). The aliquots were loaded directly on to 1% agarose gel and electrophoresed at 90 V in 1×TAE buffer. The gel was stained with 0.5 mg L^{-1} ethidium bromide and then bands were visualized by photographed under

UV illuminator. After electrophoresis, the proportion of DNA in each fraction was estimated quantitatively from the intensity of the bands using AlphaDigiDoc™ RT. Version V.4.0.0 PC–Image software. The degree of DNA cleavage activity was expressed in terms of the percentage of conversion of the SC-DNA to OC-DNA equation describe in literature.[38]

3 | RESULTS AND DISCUSSION

3.1 | Magnetic moments, UV-vis spectral analysis and molar conductivity (Λ_m) measurements

The room temperature magnetic moments show that the binuclear Pt^{II} complexes are diamagnetic in nature. The magnetic susceptibility ($\mu_{eff.}$) values indicate a pairing of electron with low-spin t_2g^6 eg^2 configuration. Pt^{II} complexes have square planer geometry i.e. dsp^2 hybridisation. Which can be confirmed by electronic spectral data. The dz^2 orbital is in lowest energy state compare to dx^2-y^2 orbital energy state for Pt^{II} complex. UV-vis spectra of homoleptic Pt^{II} complexes (Figure 1) show three bands in range of 294–472 nm. The highest wavelength (d–d transition) band is observed at 470–472 nm region. The bands in the region 357-360 nm and 294-309 nm are assigned to MLCT (Metal to ligand charge transfer) and ILCT (Intra ligands charge transfer) transitions, respectively.[39,40] The molar conductivity (Λ_m) values of Pt^{II} complexes are observed in the range of 18 – 25 $\Omega^{-1}cm^2mol^{-1}$, which suggests the non-electrolytic nature of the complexes.

3.2 | EDX, ^{1}H NMR and ^{13}C NMR

Energy dispersive X-rays analysis (EDX) data (Figure 2) for the binuclear Pt^{II} complex 6a confirmed the weight % of C, N, O, S, Pt and Cl as 27.49, 6.34, 2.0, 4.36, 41.93, 16.05, respectively, as estimated with the calculated values 28.83, 6.11, 1.75, 3.50, 42.58, 15.47, respectively. The elemental analysis data of the synthesized ligands (5a-5f) are represented in supplementary material 1. ^{1}H NMR spectra of all synthesized compounds exhibit a peaks in the range of δ 7.00-9.00 ppm assigning aromatic protons. The ^{1}H NMR spectra of complexes are shifted to down field compare to corresponding fused heterocyclic pyrazolo[1,5-a]pyrimidine nucleus based ligands (5a-5f). ^{1}H NMR spectra of compounds (5a-5f and 6a-6f) are represented in supplementary material 2 whereas spectral data in experimental section.

In the ^{13}C NMR spectrum, the signals for (-C, -CH) aromatic carbons appears between 167 and 105 ppm, respectively. The C4 carbon of ligands (5a-5f) gave an intense singlet at about 94.00-95.00 ppm, it is shifted to 120-121.50 ppm in the spectra of complexes (6a-6f) suggest formation of complex. ^{13}C NMR spectra (5a-5f and 6a-6f) are represented in supplementary material 3 whereas spectral data in experimental section.

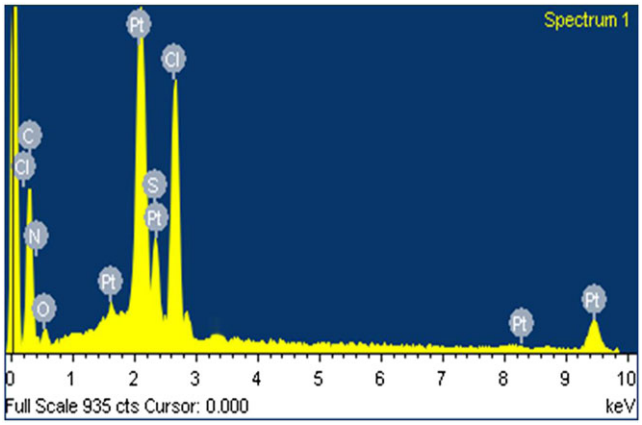

FIGURE 2 EDX spectrum of the Pt^{II} complex 6a

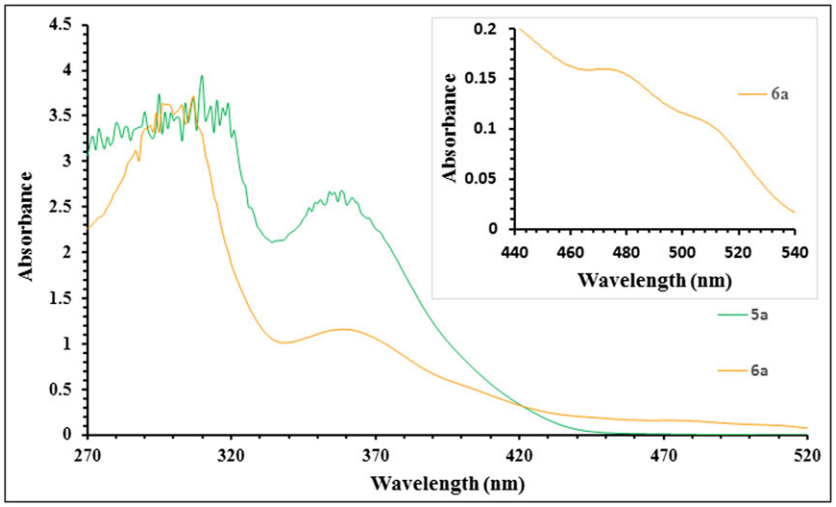

FIGURE 1 Electronic spectrum of ligand 5a and Pt^{II} complex 6a

3.3 | FT-IR characterisation

A primary effort was made for the characterization of the synthesized compounds by FT-IR spectroscopy. IR spectra of free N-aza heterocyclic pyrazolo[1,5-a] pyrimidine based compounds, are an illustration in supplementary material 4 and spectral frequency bands are represented in experimental section. While pyrazolo[1,5-a] pyrimidine derivatives (neutral -N,-S & -N,-N donor tetradentat) of ligands are capable to coordinate with platinum metal to form chelating five membered ring in Pt^{II} complexes. Infrared spectra of the pyrazolo[1,5-a] pyrimidine derivatives ligands exhibit few functional groups i.e. azo methine (>C=N) group of pyrazolo[1,5-a]pyrimidine and pyrimidine moiety, (>C=C<) group of conjugated aromatic alkene and (C-S-C) of thiophene functionality. The azo methine stretching vibrations ν(C=N), in a N-aza heterocyclic pyrazolo[1,5-a] pyrimidine derivatives ligands are observed frequency in the range of 1704-1710 cm^{-1} and in complexes its shifted to lower wavenumber (80-90 cm^{-1}) at 1604-1566 cm^{-1}, which exhibits that azo methine group coordinated to metal ion by chelation.[41,42] The band ν(C-S-C) of the sulphur containing heterocyclic five membered ligands are observed in the range of 1080-1087 cm^{-1}, and thiophene ring coordinate with Pt^{II} metal ion to form complexes, the frequency appear in range of 1018-1021 cm^{-1}, which indicate the band of complexes are shifted to (60-70 cm^{-1}) lower frequency as compared to ligands. N-aza heterocyclic pyrazolo[1,5-a]pyrimidine moiety contain nitrogen atom coordinates with Pt^{II} metal ion forming chelative compounds, the band ν(Pt-N) observed in the range of 632-640 cm^{-1}, while thiophene ring of sulphur atom coordinate with Pt^{II} ion exhibit the band $\nu_{(Pt-S)}$ in the range of 555-570 cm^{-1}.[41] These bands are shifted to lower wavenumbers (80-90 cm^{-1}) indicating the coordination of metal through aza/sulphur in all complexes. The aromatic (C-H) band of ligands and complexes are also observed in the range of 2916-3130 cm^{-1}.[43] These spectral interpretations and their assignments are consistent with the literature data.[44,45]

3.4 | LC-MS analysis

Intensity vs mass upon charge ratio spectrum and possible mass fragmentation pattern of binuclear Pt^{II} complex (6d) are illustrated in Figure 3. Mass spectral data of free ligands (5a-5f) and platinum(II) complex (6a) are represented in experimental section. Mass spectral graphs of ligands (5a-5f) are represented in supplementary material 5. Complex (6d) shows molecular ion peaks at 928.88 m/z, 930.80 m/z, 932.49 m/z, 934.79 m/z and 936.38 m/z are assigned to [M], [M+2], [M+4], [M+6] and [M+8], respectively, due to the presence of four chlorine atom in the complex 6d. The peak observed at 789.01 m/z value, is due to the loss of four chlorine atoms. The peak at 399.08 m/z is due to the loss of two platinum metal ions, which is due to 7-(4-nitrophenyl)-5-(pyridin-2-yl)-2-(thiophen-2-yl)pyrazolo[1,5-a]pyrimidine ligand. The peak observed at 317.09 m/z value is due to the removal of the thiophene ring. The peak at 240.06 m/z is due to the removal of the pyridine ring. The peak at 119.05 m/z is due to removal of the nitrobenzene ring corresponds to the pyrazolo[1,5-a]pyrimidine nucleus.

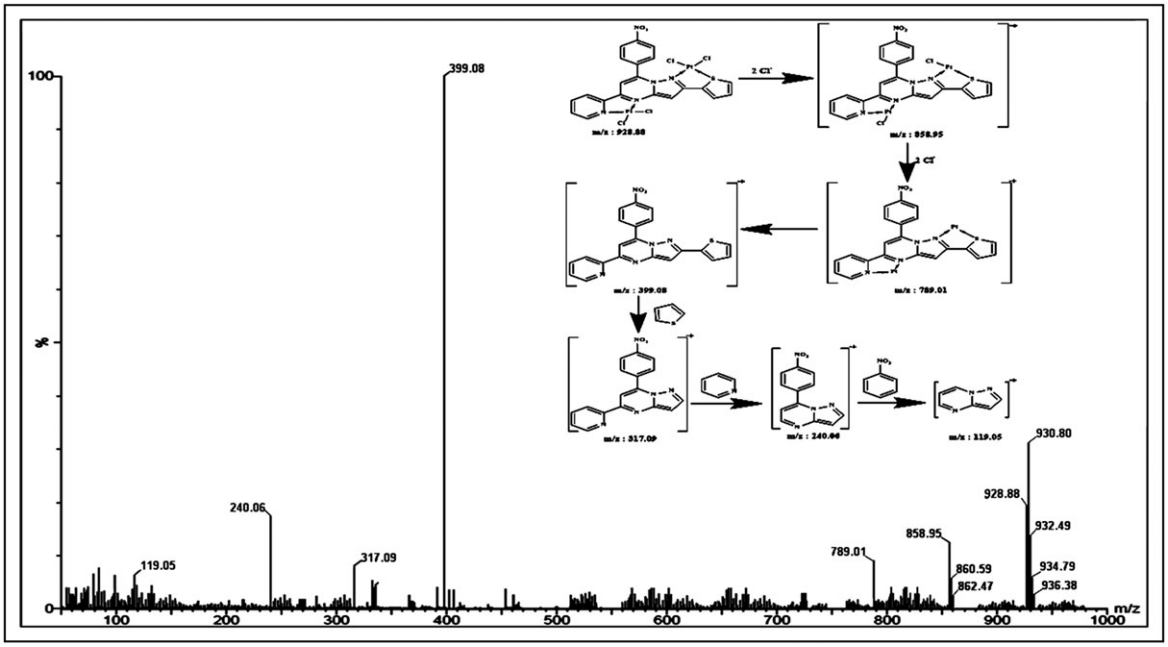

FIGURE 3 LC-MS spectrum and fragmentation pattern of Pt^{II} complex 6d

3.5 | Thermal properties

Thermogravimetric analysis (TGA) of Pt^{II} complexes was carried out under a dinitrogen atmosphere with mass eliminate due to heating system of 10 °C per minute from ambient temperature at 30 - 800 °C, the result of TGA curve (mass loss% to temperature in ^{0}C) of complex (6a) are represented in supplementary material 6. TG curve is concerned with the change in molecular weight of a compound with change in temperature. The important information that can be obtained by TGA, that there is the amount of weight loss of the compound by heating. For any complexes, the loss of water molecule from lattice sphere is observed up to 120 °C, while the coordinated water molecules directly bonded to platinum metal are eliminate at higher temperatures in between 120-180 °C, but here no mass losses occur up to 200 °C, that indicate the absence of the lattice or coordinated water molecules in the complexes. The thermogram of compound $[Pt_2(5a)(Cl_4)]$ (6a) shows the weight loss occurs in between temperature 230 - 290 °C (weight loss of 15%), which is attributed to the loss of chlorine molecules, mass loss occurring in range of temperature 300 - 550 °C (weight loss of 42%) is due the loss of ligand (5a) and leaving behind metallic platinum as a residue.[4]

3.6 | Pharmacology

3.6.1 | *In vitro* antimicrobial study

A comparative study of *in vitro* antimicrobial screening indicates that binuclear Pt^{II} complexes showed greater activity against Gram$^{(-ve)}$ and Gram$^{(+ve)}$ bacteria, when pyrazolo[1,5-a]pyrimidine ligand incorporated. The results concerning MIC values of the compounds and standard drug such as gatifloxacin (GFLH), ciprofloxacin (CFLH), levofloxacin (LFLH), norfloxacin (NFLH), ofloxacin (OFLH), pefloxacin (PFLH) and sparfloxacin (SFLH) are represented in Figure 4 and supplementary material 7. Complex (6d) exhibits the excellent potency amongst all the complexes due to the presence of the highly electro withdrawing power of the nitro ($-NO_2$) substituted on phenyl ring, its enhance the biological study.[46] Additionally, the heights activity of nitro substituent with complexes are high lipophilic in nature, that the complexes penetration through cell membrane due to their increase in lipophilicity. Antibacterial activities include inhibition of cell wall synthesis, functions of cellular membrane, protein synthesis, nucleic acid synthesis and folic acid synthesis in stepwise manner. MIC values of complexes are increasing due to chelation. This effect can be explained by

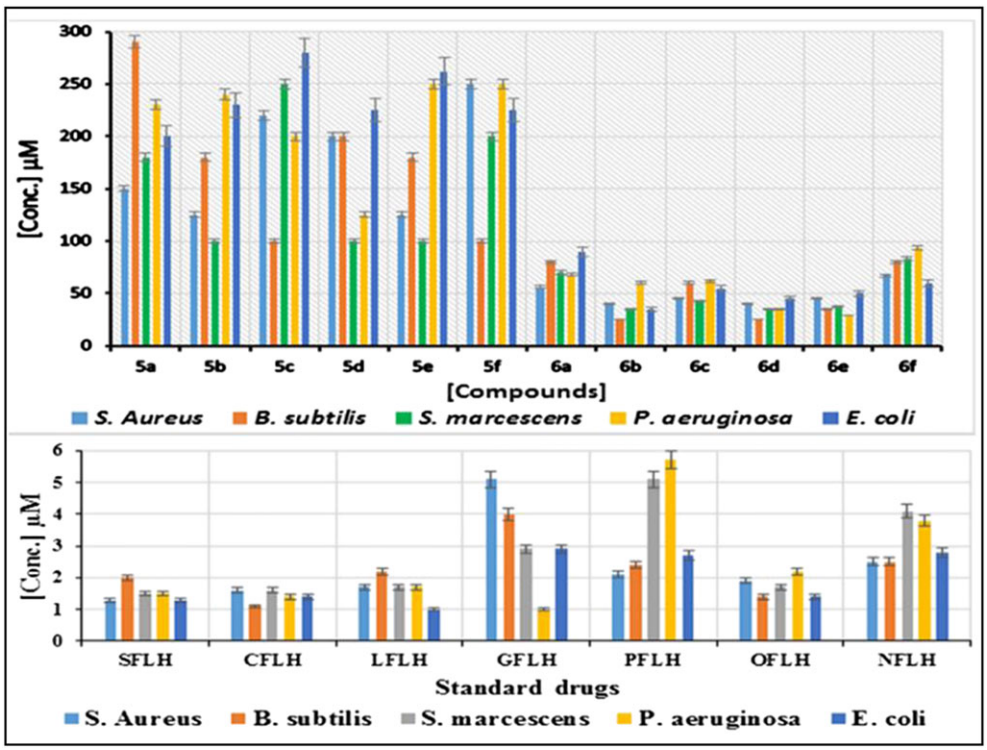

FIGURE 4 Effect of different concentrations of ligands, Pt^{II} complexes and standard drugs (Gatifloxacin (GFLH), ciprofloxacin (CFLH), levofloxacin (LFLH), Norfloxacin (NFLH), Ofloxacin (OFLH), Pefloxacin (PFLH) and Sparfloxacin (SFLH) on five different pathogens. Error bars represent the standard deviation of three repeats

chelation that make possible the ability of a complex to cross a cell membrane, which can be also explained by Tweedy's chelation theory.[47–49] Therefore, we favour that the toxicity of the complexes can be associated to the strengths of the metal-ligands bond, and furthermore, other factors such as size of the cation, and receptor sites.

3.7 | Cellular level bioassay using *S. pombe* cells

Schizosaccharomyces pombe cells were used to study toxic effect of compounds in the biological metabolism.[46,50] A relative study of cytotoxicity effect of heterocyclic compounds and their metal complexes indicate that the metal complexes exhibit better cytotoxicity compare to corresponding pyrazolo[1,5-a]pyrimidine ligand. Sensitive and selective cells can interact with the compounds and can be easily monitored by trypan blue dye. Trypan blue dye did not penetrate to living *S.pombe* cells because of its cell membrane cannot be destroyed, while it can penetrate to dead cell of *S. pombe* as a result blue colour under microscope is observed (Figure 5). The toxicity is found to be differ with the type of substituent present in the synthesized compounds. After 17-20 h of the treatment, many of the *S. pombe* cells are destroyed due to the toxic nature of the compound.[47] Cytotoxicity activity of all complexes are higher than their respective free ligands and are comparable with cisplatin and transplatin.[51] Complexes (6d, 6b, 6c) are the most active amongst all the compounds due to presence of electron withdrawing substituents (-NO_2, -F, Cl). Overall vconclusion is that as concentration of compounds increases cellular level cytotoxicity also increases. The percentage viability of compounds are represented in Figure 6 and cytotoxicity data of the compounds are shows in supplementary material 8.

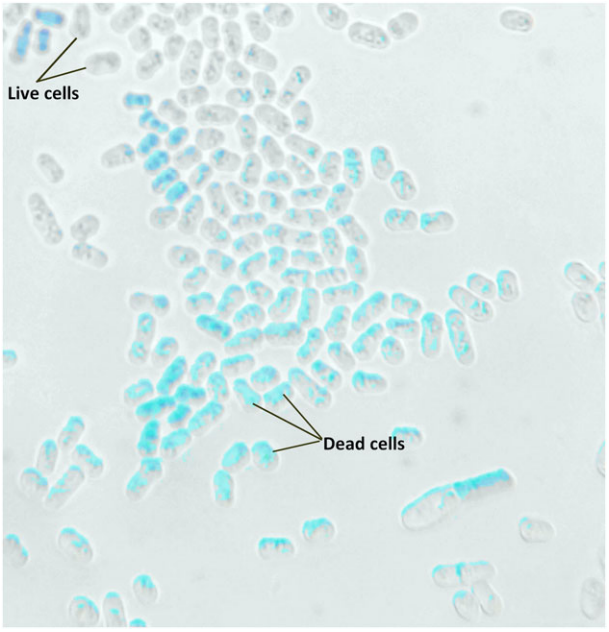

FIGURE 5 Effect of compounds on *S. pombe* cells. Dead cells are blue colour, whereas live cells are transparent

3.8 | Effect of platinum(II) complexes (6a-6f) on the degradation of DNA of *S. pombe* cells

The results of *in vivo* cytotoxicity against eukaryotic cell stimulated us to discover whether the complexes have any influence on the degradation of DNA or not. The conclusion of the synthesized complexes (6a-6f), the DNA degradation of *S. pombe* cells was approved by the separation of DNA from treated and untreated *S. pombe* cells and also DNA degrade of the *S. Pombe* cells is visualised by electrophoresis on 1% agarose gel. DNA destroyed establish as smear in platinum(II) complexes treated with *S. pombe* cells, while in untreated *S. pombe* cells, entire band have no smearing. The results of complexes (6a-6f) of the degradation of *S. Pombe* cells DNA represented in Figure 7. Smearing of *S. Pombe* cell of DNA concluded that the damage has followed due to lethal nature of the compounds. The cellular level cytotoxicity result is in agreement with that platinum(II) complexes have entered into the *S. Pombe* cell and affected the degradation of DNA. Cisplatin, transplatin and platinum(II) complexes are more cytotoxic potency as compared to pyrazolo[1,5-a] pyrimidine derivatives ligands.

3.9 | *In vitro* cytotoxicity bioassay

Synthesized compounds were screen for their cytotoxicity using the protocol of Meyer *et al*. [50,52] This cytotoxic process is inexpensive, less time consuming and consistent. LC_{50} value is calculated from the plot of the log concentration of compounds vs LC_{50} values. Antilog of the obtained value at 50% fatality gives the value of LC_{50}. From the graph, the LC_{50} values of the synthesized compounds are calculated and they are found in the range of 6.450 - 102.07 μg/ml. Complex (6b) is more potent compare to other complexes and corresponding ligands (Figure 8). The order of potency of compounds is cis-platin > 6d > 6b > 6c > 6a > 6e > 6f > trans-platin > pyrazolo[1,5-a] pyrimidine derivatives ligands.[46] Particularly, the complexes 6b, 6d and 6c exhibit high potency due to their high electro–withdrawing substitution and less sterically hindered on the ligand. The LC_{50}

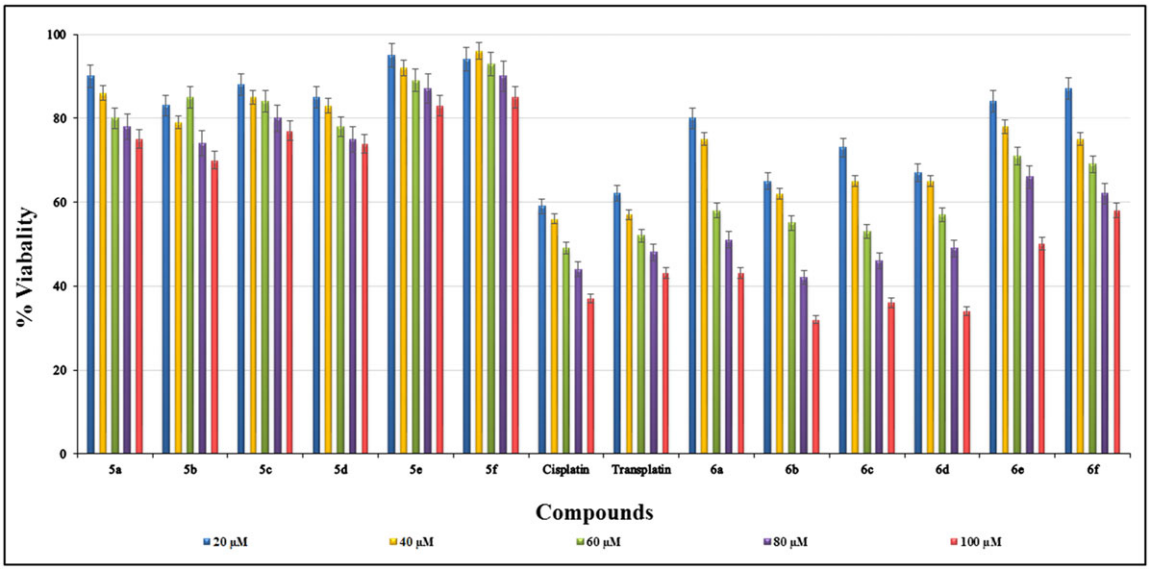

FIGURE 6 The percentage viability of compounds at different concentrations with error uncertainty in the value ±5%

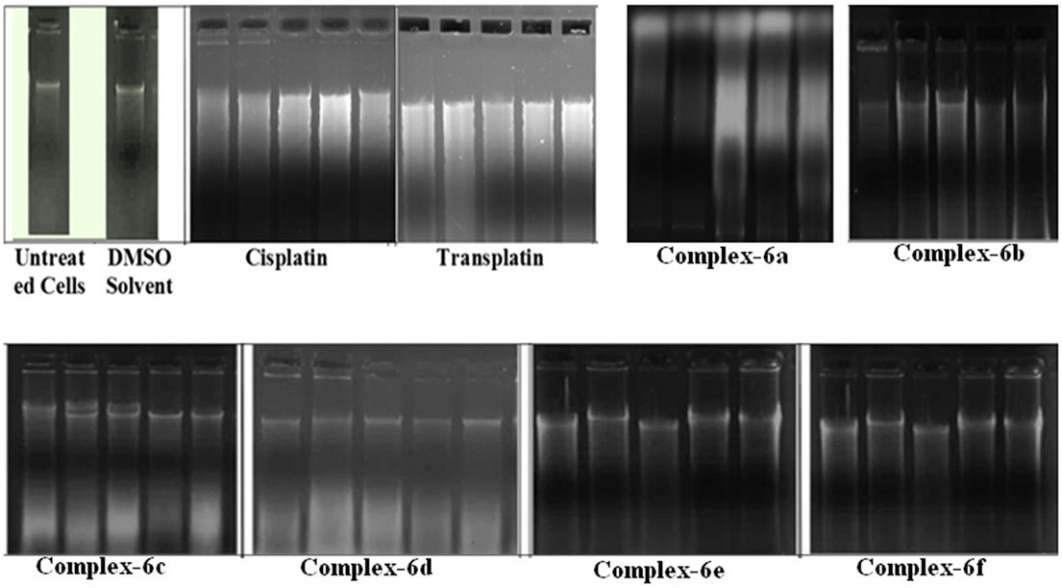

FIGURE 7 Lane 1-5 represent the DNA damage of the *S. pombe* cells by the treatment of platinum(II) complexes **(6a-6f)** in the range of (20 – 100 μM) while lane untreated represents *S. pombe* cells as the control and another lane DMSO solvent + DNA + *S. Pombe* cells to study genotoxicity

value of all synthesized compounds are comparable to standard anticancer agent *cis*-platin and transplatin.

3.10 | *Mycobacterium tuberculosis* (Mtb) $H_{37}Rv$ strain

In vitro antituberculosis activity of the synthesized Pt^{II} complex (6d) have been screened against *Mycobacterium tuberculosis* $H_{37}Rv$ strain. The complex (6d) possess excellent activity (12.5 μg/ml) against *M. tuberculosis* $H_{37}Rv$ strain due to presence of nitro substituent on fused heterocyclic ligands. The compounds which showed higher inhibition against *M. tuberculosis* $H_{37}Rv$, are further study for their MICs.

3.11 | *In vitro* antiproliferative cytotoxicity on human colorectal carcinoma HCT-116 cells

The positive results observed in DNA binding and DNA cleavage studies have directed us to examine the cell growth inhibition of the platinum(II) complexes. To

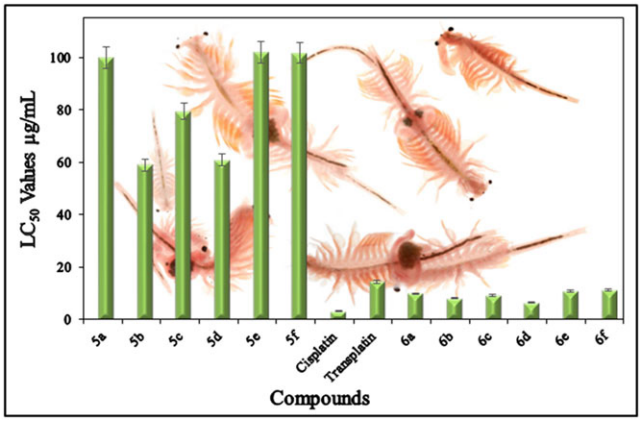

FIGURE 8 Plot of LC_{50} values of different compounds in µg L^{-1} using brine shrimp to determine the cytotoxic effects. Error bars represent the standard deviation of three replicates ± 5%

investigate the potential of the complexes as antitumor agents, *In vitro* antiproliferative assay of the synthesized platinum(II) complexes (6a-6f) against Human Colorectal Carcinoma HCT-116 cell line were evaluated by MTT assay. The concentration of platinum(II) complexes are taken in the range of 10-1000 µg/ml. The viability of cells in the presence of the tested compounds is compared to that observed in control cultures and the inhibition of growth (%) is calculated. The IC_{50} (i.e., the concentration producing 50% inhibition of growth) is determined and expressed in µg/ml concentration (Figure 9). The IC_{50} values of the platinum(II) complexes (6b, 6c and 6d) exhibit a certain inhibitory effect on HCT-116 cancer cell line, while platinum(II) complexes (6a, 6e and 6f) are found to be practically ineffective. Pt^{II} complexes (6b -F, 6c -Cl and 6d -NO_2) containing electron withdrawing functional group are greater *in vitro* cytotoxicity than the complexes (6a –OCH_3, 6e –CH_3 and 6f -H) containing electron releasing group. Furthermore, the IC_{50} values of the Pt^{II} complexes (6b, 6c and 6d) are comparable with standard drug such as cisplatin (51.64 µM)[53], carboplatin (273.05 µM) and oxaliplatin (57.04 µM).[27] IC_{50} value of the complexes 6b, 6c and 6d are comparable to the standard drugs cisplatin and oxaliplatin. Complexes (6d –NO_2 and 6b –F) are the most cytotoxic against HCT-116 cancer cell line as compared to other complexes. To found the effect of DMSO on the cells' viability, control solutions with the respective DMSO content are also screened and the cytotoxic effect of DMSO is very low. The IC_{50} value of the Pt^{II} complexes are found in increasing order of 6d (182.93 µM) > 6b (320.36 µM) > 6c (325.52 µM) > 6a (344.73 µM) > 6e (674.15 µM) > 6f (> 1000 µM) > DMSO.

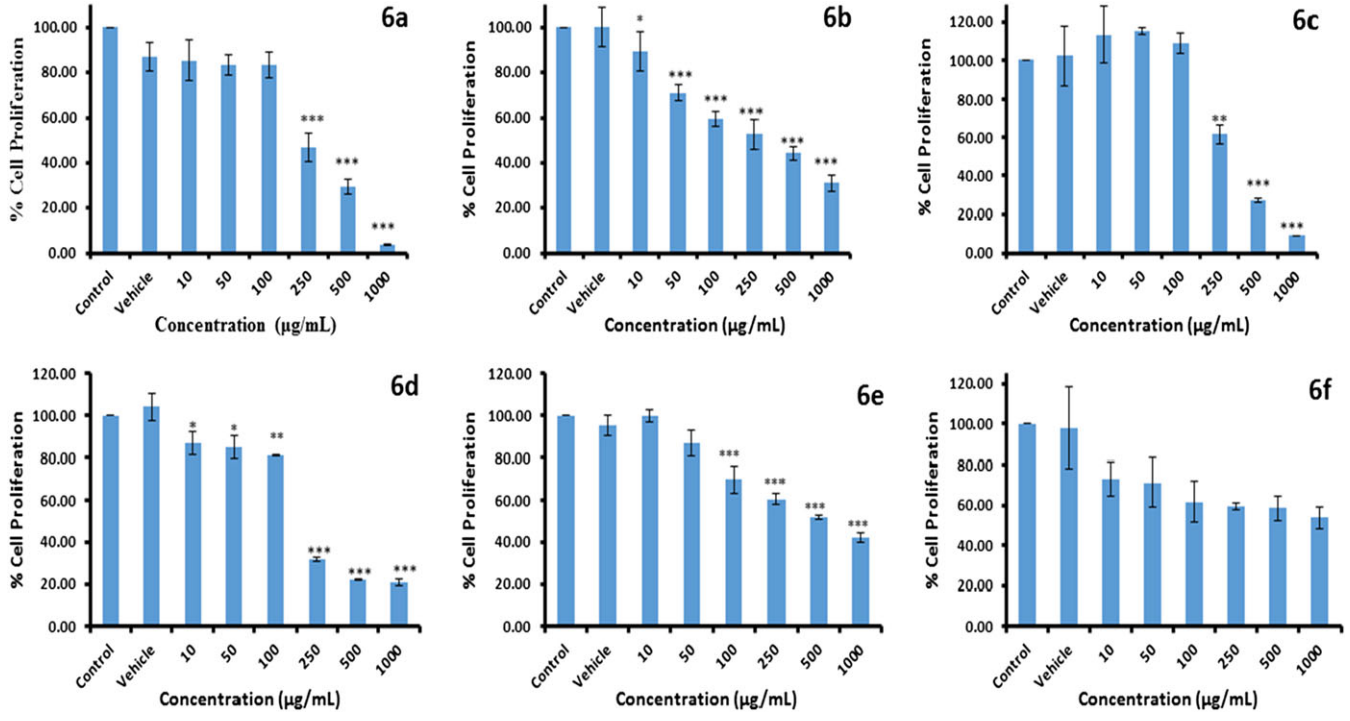

FIGURE 9 Effect of synthesized Pt^{II} complexes conjugate on cell proliferation. Determination of IC_{50} values of Pt^{II} complexes (6a–6f) conjugate in HCT 116 cells. HCT 116 cells were treated with the various concentrations control (100% DMSO), vehicle control (0.5% DMSO), 10, 50, 100, 250, 500, 1000 µg/mL) of Pt^{II} complexes (6a–6f) conjugate for 24 h. MTT assay determined inhibition of HCT 116 cells. The obtained values were plotted and the IC_{50} values were analysed the data with t-test using Sigmaplot 12.0. Note: Error bars represent standard deviation of three replicates

3.12 | Structure–activity relationship (SAR)

The biological activity is significantly affected by introducing six-different (-OCH_3, -F, -Cl, -NO_2, -CH_3, -H) substituted phenyl ring at C-8 position, thiophene ring at C-3 position and pyridine ring at C-6 position on pyrazolo[1,5-a]pyrimidine scaffold (Figure 10). It is observed that the highly electron withdrawing nitro substituent in phenyl moiety at C-8 position in pyrazolo[1,5-a]pyrimidine core (compound 6d) exhibit higher antituberculosis assay against *Mycobacterium tuberculosis* H_{37}Rv strain as compared other compounds (6a, 6c, 6b, 6e, 6f) and also enhanced antibacterial activity against Gram$^{(-ve)}$ bacterial species. The replacement of electron donating substituents with methoxy group (6a), methyl group (6e) and hydrogen group (6f) at *para*-position on phenyl moiety decreases the antibacterial activity against *P. aeruginosa* and *E.coli*, while the electron withdrawing chloro group (6c) and nitro (6d) and fluoro (6b) group exhibit highest activity against *S. marcescens* and *B. subtilis,* respectively. The complexes (6b, 6c, 6d) show excellent cytotoxicity against *S. pombe* cells, *in vitro* brine shrimp cytotoxicity and HCT-116 cancer cell line cytotoxicity as compared to other complexes (6e, 6a, 6f).[39] It is observed that presence of electron withdrawing substituents (-F, -Cl, -NO_2) in complexes (6b, 6c, 6d) increased antimicrobial activity. The pyrazolo[1,5-a] pyrimidine nucleus with nitro substituent at *para*-position on phenyl moiety at C-8 position, exhibits moderate antituberculosis activity against *Mycobacterium tuberculosis* H_{37}Rv strain as compared to isoniazid and rifampicin drugs. The existence of electron releasing group (-OCH_3, -CH_3 and -H) at *para*-position in phenyl moiety decreased antibacterial potency and also decrease toxicity against *S. pombe* cells and brine shrimp lethality bioassay.

3.13 | DNA interactions studies

3.13.1 | By electronic absorption titration

Quantitative binding strength of the complexes have been carried out by electronic absorption titration (Figure 11). Electron rich (Lewis bases) biomolecule compound is bound to the electron deficient Pt^{II} complexes. Electronic absorption titration technique gives good evidence of the complex-DNA interaction and also measured for binding mode and binding strength of the

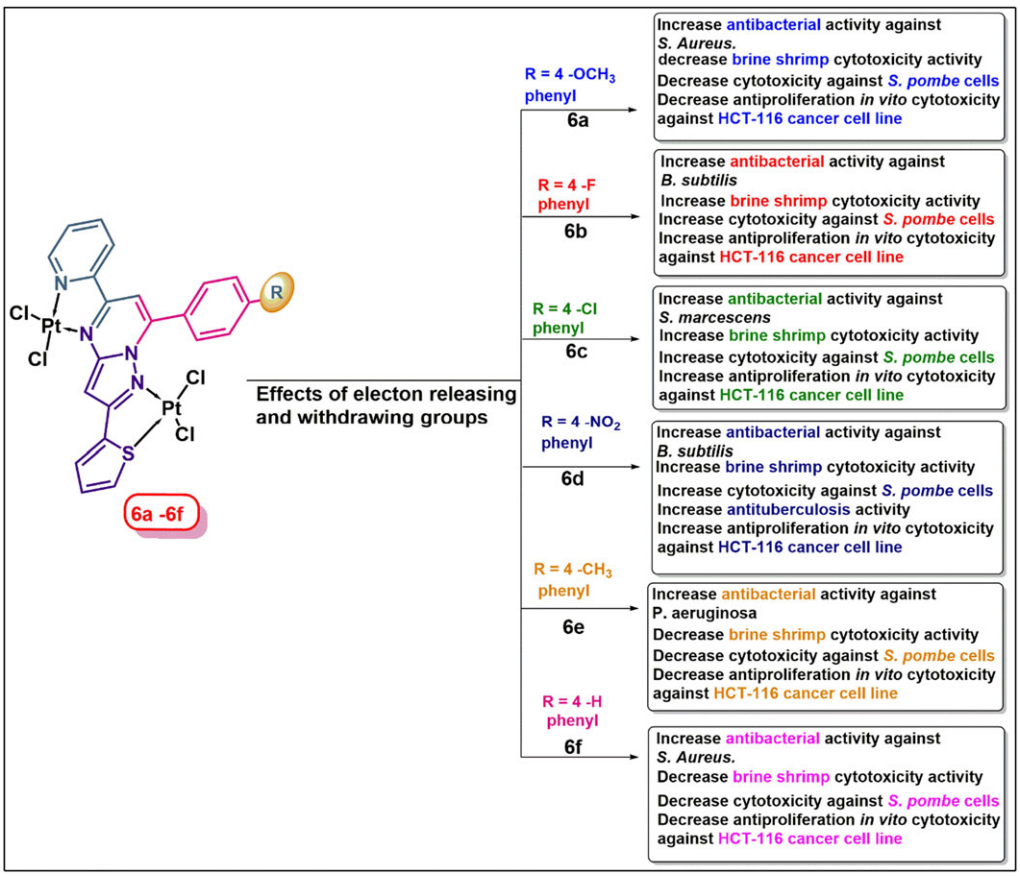

FIGURE 10 Structure–activity relationships for inhibitory concentration (IC_{50}) and lethal concentration (LC_{50}) values of the synthesized compounds

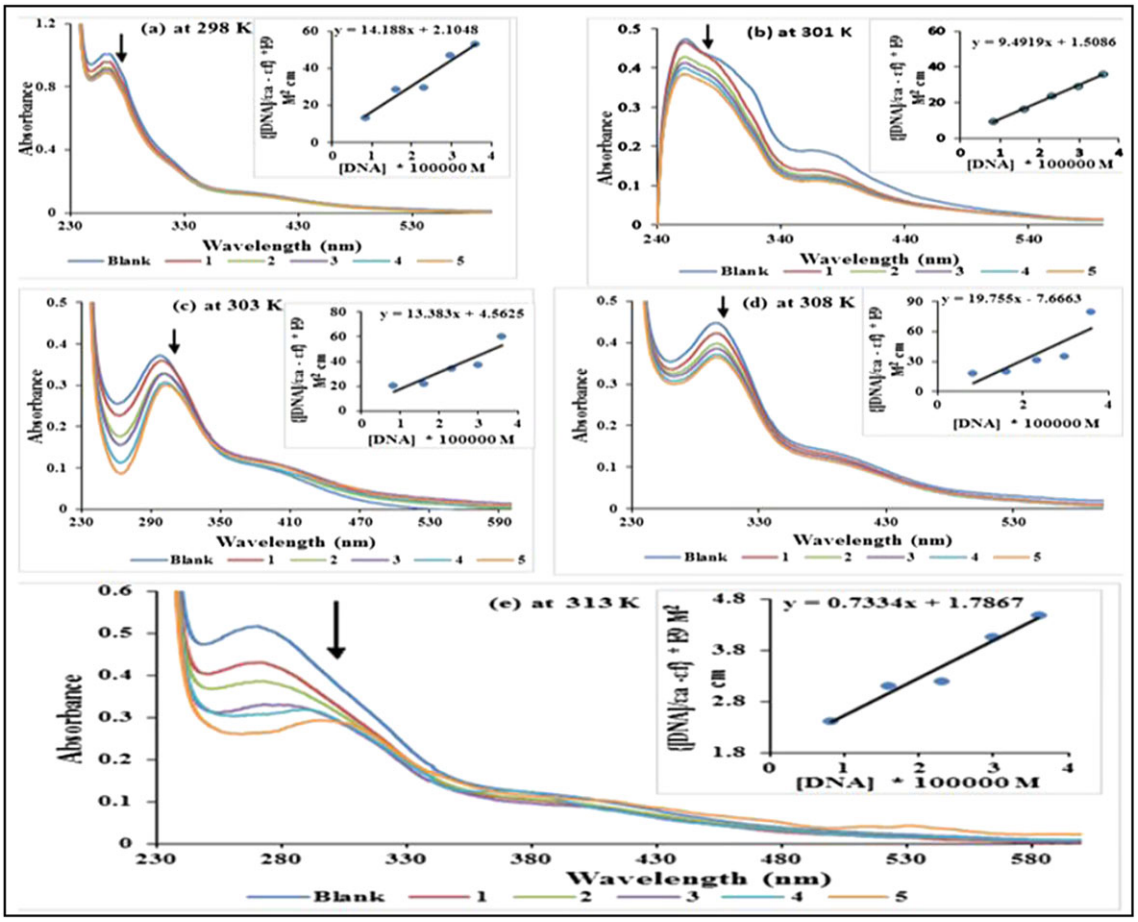

FIGURE 11 Absorption spectral changes upon addition of HS DNA to the solution of Pt^{II} complex (6d) after incubating it for 10 minutes at five different temperature (a) at 298 K (b) at 301 K (c) at 303 K (d) at 308 K (e) at 313 K in phosphate buffer (Na_2HPO_4/NaH_2PO_4, pH = 7.2). Inset: Plot of [DNA]/ (εa-εf) *vs.* [DNA]

complex-DNA adduct. The overall binding constants, (K_b) of the complexes to HS DNA, are quantitatively determined by observing the changes in the absorption intensity of the spectral bands by successive addition of HS DNA at different temperatures as represented in Figure 10. There are mainly two binding modes for the drug or complex-DNA interaction. (I) covalently binding (ii) non-covalently binding mode. In covalent binding mode, complexes that undergoes fast substitution reaction take place that means the labile group of Pt^{II} compound is replaced by a N7 position of the sugar. The Pt^{II} complexes, along with most drugs tend to interact with DNA non-covalently through three selective modes: intercalative, electrostatic (binding to the phosphate group) and groove binding.[54] The interaction affinity of the complex-DNA led to a decrease in hypochromism with a slight bathochromic shift at 2-4 nm.[55,56] This spectral study suggests stacking interaction between the aromatic conjugated cyclic compound and DNA base pairs.[57]

The calculated binding constant (K_b) of the Pt^{II} complexes with DNA are found in the range of 0.23-6.74 × 10^5 M^{-1} indicating that the complexes show an effective DNA binding ability. It is lower than the K_b value of the classical intercalator (EB) ethidium bromide (7.16 × 10^5 M^{-1}) and have higher binding affinity compared to the cisplatin (5.73 × 10^4 M^{-1}),[58] oxaliplatin (5.3 × 10^3 M^{-1})[59] and carboplatin (0.33 × 10^3 M^{-1}).[60] The K_b values are found in the order of 6d > 6b > 6c > 6a > 6e > 6 f. The decrease absorption intensity and thoroughly increase wavelength suggest that the complex-DNA interaction via partial intercalative mode of binding. Complex (6d) shows the highest binding affinity as compared to the other complexes and ligands due to the existence of a nitro group.

To get additional information of complex-DNA interactions, the thermal parameters like the change in enthalpy (ΔH°), change in free energy (ΔG°), and change in entropy (ΔS°) changes are calculated by using the Van't Hoff equation 4 and 5.[61] The K_b and thermal parameters are represented in Table 1.

$$\ln Kb = -\frac{\Delta H^{\circ}}{RT} + \frac{\Delta S^{\circ}}{R} \tag{4}$$

$$\Delta G^{\circ} = \Delta H0 - T\Delta S^{\circ} \tag{5}$$

TABLE 1 The binding constant (K_b) and thermodynamic parameters (ΔH^0, ΔS^0 and ΔG^0) for the interaction of Pt^{II} complexes with DNA at five different temperatures

Compounds	λ_{max} (nm) Bound free	Δλ (nm) red shift	T (K)	$K_b \times 10^5$ (M^{-1})	Hyper. (%)	ΔH^0 (kJ mol^{-1})	ΔS^0 (J mol^{-1} K^{-1})	ΔG^0 (J mol^{-1})
6a	308 305	3	298	3.82	21.56	-106.7	-254.059	-31,033.80
	265 264	1	301	1.64	19.12			-30,271.62
	308 306	2	303	1.06	23.63			-29,763.50
	310 306	4	308	0.51	18.02			-28,493.21
	310 312	2	313	0.47	27.83			-27,222.91
6b	299 297	2	298	4.11	39.27	-158.8	-422.784	-32,882.73
	284 280	4	301	3.67	19.78			-31,614.38
	308 306	2	303	3.19	37.46			-30,768.82
	299 298	1	308	0.49	21.95			-28,654.90
	306 302	4	313	0.28	32.91			-26,540.98
6c	265 264	1	298	5.23	18.34	-73.15	-136.998	-32,323.63
	269 266	3	301	3.35	19.30			-31,912.64
	306 305	1	303	2.33	20.98			-31,638.64
	266 265	1	308	1.91	17.59			-30,953.65
	270 268	2	313	1.14	18.34			-30,268.66
6d	266 265	1	298	6.74	17.78	-141.4	-360.645	-33,949.02
	263 261	2	301	6.29	20.12			-32,867.09
	303 299	4	303	2.93	19.35			-32,145.80
	297 296	1	308	2.58	18.34			-30,342.57
	286 275	9	313	0.41	42.55			-28,539.35
6e	310 306	4	298	4.79	21.87	-89.20	-192.161	-31,936.78
	308 306	2	301	2.45	23.23			-31,360.30
	313 308	5	303	2.12	17.33			-30,975.98
	307 304	3	308	0.93	20.46			-30,015.17
	332 327	5	313	0.87	19.40			-29,054.36
6f	265 264	1	298	3.86	16.70	-106.4	-250.401	-31,832.94
	300 298	2	301	2.27	17.29			-31,081.74
	306 305	1	303	2.19	18.12			-30,580.94
	307 301	5	308	0.76	18.39			-29,328.93
	295 293	2	313	0.53	20.68			-28,076.93

Hyper.(%) = $[(A_{free} - A_{bound})/A_{free}] \times 100\%$,

K_b = Intrinsic DNA binding constant determined from the UV-vis absorption spectral titration,

T = Temperature in kelvin (K),

ΔH = Change in enthalpy,

ΔS = Change in entropy,

ΔG = Gibb's free energy,

Δλ = Difference between bound wavelength and free wavelength.

where, K_b is at the corresponding temperature (T), and value of gas constant (R) is 8.314 $Jmol^{-1}$ K^{-1}. The Van't Hoff plots for the interaction are shown in Figure 12. The negative values of change in Gibb's free energy (ΔG°) indicate a spontaneous interaction of the complex-DNA, while the positive values of the change in enthalpy (ΔH°) and change in entropy (ΔS°) indicate that the binding between the complex-DNA is mainly hydrophobic in nature.[39,62] Furthermore, the K_b decrease with the increasing temperature of the complexes. The K_b values are calculated at different temperature, such as 298, 301, 303, 308 and 313 K. The binding mode of the complexes are further conformed by viscosity measurements and fluorescence quenching analysis.

3.14 | Viscosity measurement

Pt^{II} complexes are coordinated with N7 position of base pairs (A = T and G≡C) on DNA through intercalation, partial intercalation, electrostatic interaction and groove

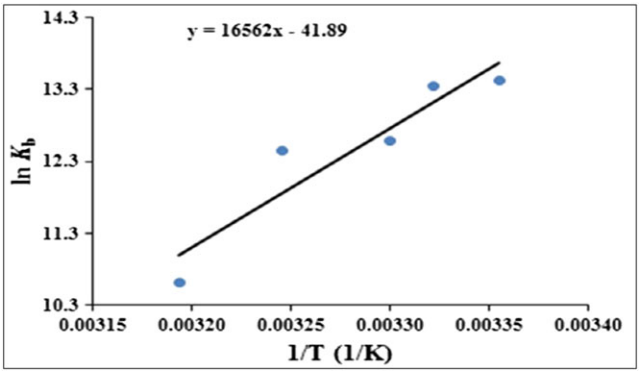

FIGURE 12 The Van't Hoff plot of Pt^{II} complex (6d) at different temperatures

binding. The relative viscosity curve of complexes are represented in Figure 13. The plot of relative viscosity is a $(\eta/\eta^0)^{1/3}$ vs the ratio of the decrease concentration of the complex-DNA solutions. Increasing concentrations of complexes (6a-6f), relative viscosity of the HS-DNA solutions steadily increases, suggests the intercalative binding mode. Complex 6d shows increase in relative viscosity due to presence of electron withdrawing ($-NO_2$) functionality. Increase in viscosity values shows affinity of compounds to bind with DNA, which follows the order 6d > 6b > 6c > 6a > 6e > 6 f. Results conclude that complexes show partial intercalation binding with DNA base pairs, which is consistent with our interpretation based on binding constants.

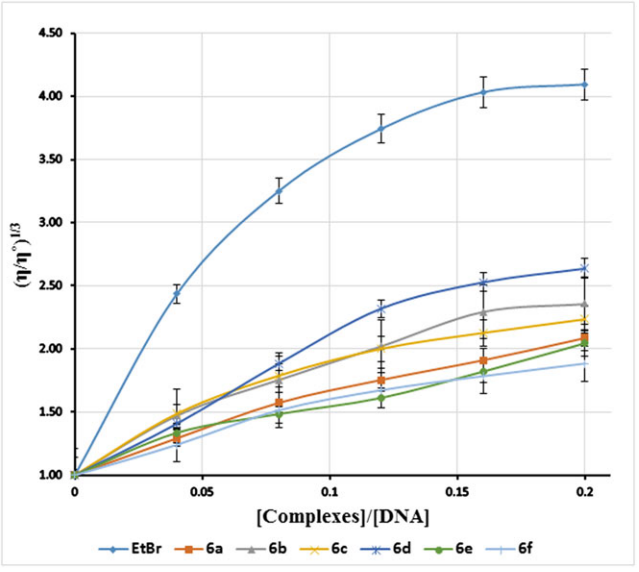

FIGURE 13 The effect of increasing amounts of complexes on the relative viscosity of HS-DNA at 27 (±0.1) ^{0}C in phosphate buffer at pH = 7.2. Error bars represent the standard deviation of three replicates

3.15 | Molecular docking with DNA

Molecular docking study played important roles in the molecular recognition of nucleoside and nucleotide in the rational design of new chemotherapeutic drugs. Docking study of complex-DNA performed in order to predict the binding site along with desired orientation of the molecules inside the DNA.[34] Docking structure of the complex (6d) is illustrate in Figure 14 and other docking structure of Pt^{II} complexes and ligands are illustrate in supplementary material 9. The binding energies of docking structure of ligands (5a-5f) and complexes (6a-6f) are found to be -257.45 **(5a)**, -271.89 **(5b)**, -275.50 **(5c)**, -265.96 **(5d)**, -256.06 **(5e)**, -268.07 **(5f)**, -287.88**(6a)**, -275.07 **(6b)**, -238.75 **(6c),** -280.51 **(6d)**, -291.06 **(6e)**, -275.12 **(6f)** kJ mol^{-1}, respectively. The DNA binding energy of the compounds is negative, which with an increase the binding affinity of complex-DNA. The molecular docking study is also confirmed by electronic absorption titration, fluorescence quenching analysis and viscosity measurements studies that the complex-DNA interaction take place through the partial intercalative mode of DNA binding.

3.16 | Competitive displacement assay

For confirmation of partial intercalative mechanism, fluorescence quenching study was performed at ambient temperature. The complexes are not fluorescent in addition of the HS-DNA. Therefore, binding assay of complex-DNA cannot carried out directly through emission spectra. The planar phenanthridine ring of EB can intercalate between adjacent DNA base pairs. This intercalative mechanism suggests the intense fluorescence emission band at 610 nm and excitation wavelength at 480 nm due to fluorescence quenching and EB-DNA interaction, respectively. Within this context, the compound which can intercalate to DNA equally or more strongly than EB (typical intercalator), is added into a solution of the EB–DNA compound.[63] The addition of complexes (6a-6f) at diverse r- values resulted in a significant gradually decrease of the intensity of the emission band of the DNA–EB system at 610 nm indicating the competition of the Pt^{II} complexes with EB in binding to DNA. The observed quenching of DNA–EB fluorescence by the compounds proposes that the complexes can significantly displace to ethidium bromide (EB) from the DNA–EB system, thus the illuminating the partial interaction with HS-DNA by the intercalative mode.[64,65] The linear Stern–Volmer plots of DNA–EB for the complexes show that the quenching of EB–DNA by the complexes is in better agreement (r = 3.33) with the linear Stern–Volmer quenching equation proving that the addition of EB from

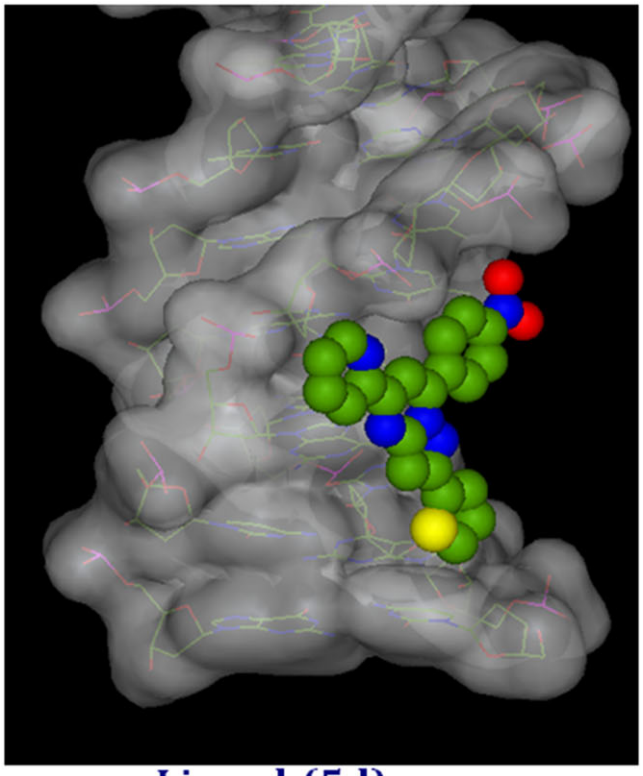

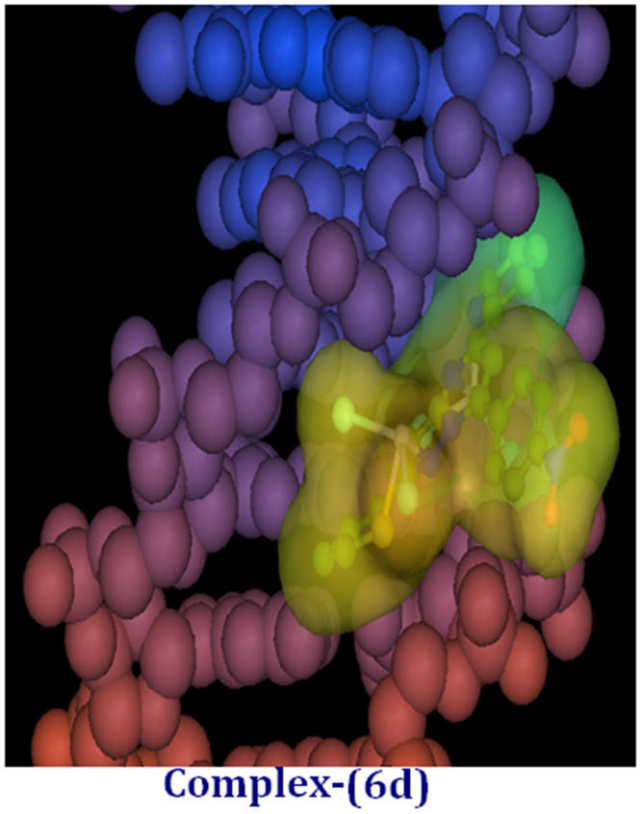

FIGURE 14 Molecular docking of ligand (5d) and complex (6d) with the DNA duplex (VDW spheres) of sequence $d(ACCGACGTCGGT)_2$. The complex and ligand are docked into the DNA base pairs (1 BNA) using hex 8.0 software

EB–DNA by each compound result in a decrease in the fluorescence intensity.[66,67] This is related to binding constant (K_a), linear Stern-Volmer quenching constants (K_{sq}), standard change in Gibb's free energy (ΔG^0) and number of compound binds with DNA (binding site, n) are represented in Table 2. The K_a values calculated from Scatchard plots indicating that complex (6c) in Figure 15, the binding constant (K_a) and linear Stern-Volmer quenching constants (K_{sq}) values of Pt^{II} complexes are found in range of $1.20 \times 10^3 - 4.20 \times 10^5$ and $3.3 \times 10^2 - 6.0 \times 10^3$, respectively. The results of fluorescence quenching data and graphs of complexes (6a-6f) are represented in supplementary material 10. The values of n is observed around 1.0 indicates the 1: 1 molar ratio between the complexes and HS-DNA.

3.17 | Gel electrophoresis

Pt^{II} complexes are in good correlation with the DNA cleavage because some of the anticancer agents approved for clinical use cause cell death by damaging DNA.[9,68] Cleavage activity on plasmid pUC19 DNA induced by synthesized Pt^{II} complexes can be observed using DNA electrophoresis. The DNA cleavage affinity of the complexes could follow by two pathway that effectively cleave of DNA molecule either with hydrolytic or oxidative pathways due to the importance of DNA nuclease in biological applications. (i) Breaking of phosphodiester moiety to further sub units can be illustrated by hydrolytic DNA cleavage study. In hydrolytic cleavage, the ability of complexes to bring about supercoil (SC) form of DNA to the open-circular (OC).[69,70] (ii) Abstracting proton of sugar (adenosine, guanine, thymine, cytosine) might lead to oxidation DNA nuclease.[71] There has been extensive interest in DNA nuclease process that are activated by metal complexes. Gel electrophoresis is an appropriate technique to evaluate the cleavage of DNA by metal based drugs, to determine the factors affecting the nucleolytic

TABLE 2 Linear stern-Volmer quenching constants (K_{sq}), number of binding sites (n), change in standard free energy (ΔG^0) and associative binding constant (K_a) of Pt^{II} complexes (6a-6f) with HS-DNA

Complexes	K_{sq} (M^{-1})	K_a (M^{-1})	n	ΔG(J mol^{-1})
6a	4.6×10^3	1.05×10^5	1.290	-28524.10
6b	3.9×10^3	1.07×10^5	1.295	-28,540.65
6c	3.3×10^2	3.71×10^4	1.011	-26,071.03
6d	6.0×10^3	1.47×10^5	1.32	-29,490.49
6e	3.6×10^3	0.91×10^4	1.11	-22,605.68
6f	1.3×10^3	1.40×10^3	1.02	-18,261.11

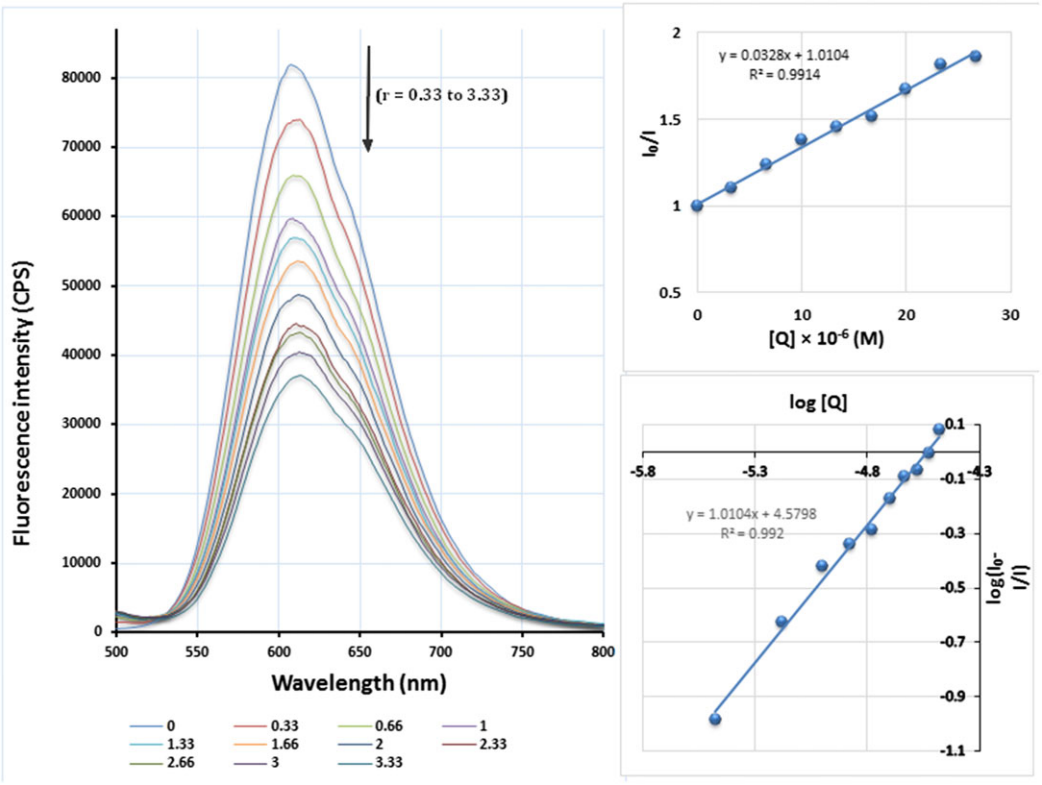

FIGURE 15 Fluorescence emission spectra of EB binds to HS-DNA in the presence of complex (6c). [EB] = 33.3 μM, [DNA] = 10 μM; [complex] = (i) 3.33, (ii) 6.66, (iii) 10, (iv) 13.33, (v) 16.66, (vi) 20, (vii) 23.33, (viii) 26.66, (iX) 30, (X) 3.33 μM; λ_{ex}= 480 nm. The arrows show the intensity changes upon increasing the concentrations of complex. Inset graph: Plots of I_0/I *versus* [Q], with • for the experimental data points and the full line for the linear fitting of the data. Comparative plot of log[I_0-I/I] *versus* log[complex] for the titration of HS-DNA EB system with complexes (6c) in (Na_2HPO_4/NaH_2PO_4, pH = 7.2) phosphate buffer medium

efficiency of a compound and to compare the nucleolytic properties of different compounds.[72]

Results of % cleavage ability of the complexes are represented in Figure 16. And data of % cleavage of Pt^{II} complexes are illustrate in supplementary material 11.

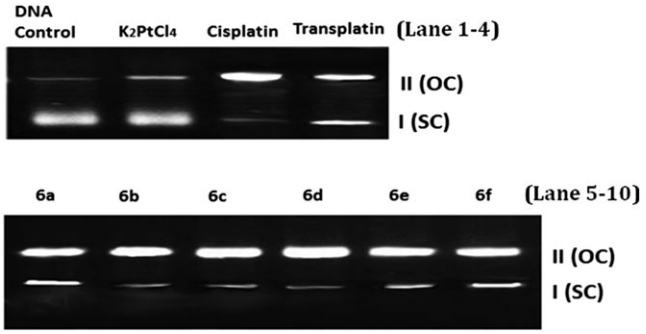

FIGURE 16 Photogenic view of the cleavage of pUC19 DNA (300 μg cm^{-3}) with a series of compounds using 1% agarose gel containing 0.5 μg cm^{-3} EtBr. All reactions were incubated in TE buffer (pH 8) at a final volume of 15 mm^3 for 3 h at 37 °C. Lane 1. DNA control, lane 2. K_2PtCl_4, lane 3. Cisplatin, lane 4. Transplatin, lane 5. (6a), lane 6. (6b), lane 7. (6c), lane 8. (6d), lane 9. (6e), lane 10. (6f)

(Figure 17) is due to the change in binding affinity of the Pt^{II} complexes to DNA. The similar behavior of Pt^{II} complexes with plasmid DNA is shown by reported compounds of the types [Pt(barb-κN)$_2$(bpy-κN,N′)],[73] [Pt(2,2′-bipyridyl-5,5′-dicarboxylic acid)Cl_2·$2H_2O$],[74] [Pt(Fc-bpa)Cl]Cl.[75] The DNA cleavage efficiency of the complexes is in order of cisplatin > 6d > 6b > 6c > 6a >

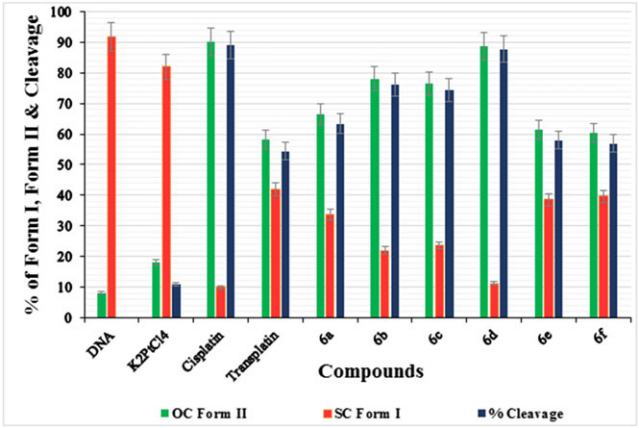

FIGURE 17 Plot of DNA cleavage data by agarose gel electrophoresis of different compounds using pUC19 DNA. Error bars represent the standard deviation of three replicates ±5%

6e > 6f > transplatin. The different DNA-cleavage efficiency of the complexes, metal salt, transplatin and cisplatin is due to the change in binding affinity of the complexes to DNA and the structural dissimilarities of ligands.

4 | CONCLUSION

In this article, a series of new pyrazolo[1,5-a] pyrimidine nuclease based ligands (5a -5f) and their Pt^{II} complexes (6a – 6f) were synthesized and characterized. And also we report the biological study of homoleptic Pt^{II} complexes (6a-6f). The complexes 6b, 6c and 6d displayed greater antibacterial activity, brine shrimp cytotoxicity and cellular level cytotoxicity against *S. pombe* cells compared to the complexes 6a, 6e, 6 f. Nitro substituted compounds 6d may be recognized as the most biologically active compound showing an interesting dual antituberculosis and antibacterial profile. All Pt^{II} complexes exhibit good antibacterial activity with low MIC values against *S. aureus*, *B.substilus* and *S. marcescens*. DNA binding of all Pt^{II} complexes observed via partial intercalative mode that confirmed by bathochromism and hypochromism of band in UV-vis absorption titration spectroscopy, increase in relative viscosity of DNA and partially decrease in fluorescence emission intensity. Complex (6d) containing nitro group is binds more strongly than the other complexes. Presence of nitro group act as not only chemical isosteres for the oxygen atoms in the heterocyclic base of thymidine, but also participate in 'strong' O–H bonding as a result it shows greater DNA binding study and antimicrobial activity, than other complexes. All the complexes and cisplatin drug show strong *in vitro* cytotoxic, as well as cellular level bioassay than transplatin. Pt^{II} complexes (6b, 6c and 6d) exhibited significant cytotoxicity against HTC-116 cancer cells and comparable to clinically used metallodrugs such as cisplatin, carboplatin and oxaliplatin. Presence of electron withdrawing group in complex 6d, 6b and 6c, improves its biological property. The preliminary studies encourage for carrying out further *in vivo* enzymatic behaviours experiments.

ACKNOWLEDGEMENTS

The authors are thankful to the Head, Department of Chemistry, Sardar Patel University, Vallabh Vidyanagar, Gujarat, India, for providing necessary research facilities, we thankful to Dhanji P. Rajani, microcare laboratory, Surat for *in vitro* antituberculosis activity, department of metallurgy. We also thankful to M.S University of baroda, for EDX analysis and DST-PURSE, Sardar Patel University, Vallabh Vidyanagar for LC-MS analysis. Authors gratefully acknowledge the University Grants Commission, New Delhi, India for meritorious fellowships awarded to them during year 2014-2018 and 'BSR UGC One Time Grant', vide UGC letter no. F.19-119/2014(BSR).

DECLARATION OF INTEREST

The authors report no conflicts of interest. The authors alone are responsible for the content and writing of the paper.

ORCID

Mohan N. Patel http://orcid.org/0000-0001-9016-9245

REFERENCES

[1] T. J. Sullivan, J. J. Truglio, M. E. Boyne, P. Novichenok, X. Zhang, C. F. Stratton, H.-J. Li, T. Kaur, A. Amin, F. Johnson, R. A. Slayden, C. Kisker, P. J. Tonge, *ACS Chem. Biol.* **2006**, *1*, 43.

[2] R. V. Ragavan, V. Vijayakumar, N. S. Kumari, *Eur. J. Med. Chem.* **2010**, *45*, 1173.

[3] A. M. Gilbert, A. Failli, J. Shumsky, Y. Yang, A. Severin, G. Singh, W. Hu, D. Keeney, P. J. Petersen, A. H. Katz, *J. Med. Chem.* **2006**, *49*, 6027.

[4] N. T. Abdel Ghani, A. M. Mansour, *Inorg. Chim. Acta* **2011**, *373*, 249.

[5] L.-L. Xu, C.-J. Zheng, L.-P. Sun, J. Miao, H.-R. Piao, *Eur. J. Med. Chem.* **2012**, *48*, 174.

[6] A. Jemal, F. Bray, M. M. Center, J. Ferlay, E. Ward, D. Forman, *CA Cancer J. Clin.* **2011**, *61*, 69.

[7] B. Rosenberg, *Naturwissenschaften* **1973**, *60*, 399.

[8] G. Hu, Y. Cai, Z. Tu, J. Luo, X. Qiao, Q. Chen, W. Zhang, *RSC Adv.* **2015**, *5*, 82050.

[9] A. Soliman, W. Linert, *Thermochim. Acta* **1999**, *338*, 67.

[10] L. Kelland, *Nat. Rev. Cancer* **2007**, *7*, 573.

[11] L. Shi, H. L. Sings, J. T. Bryan, B. Wang, Y. Wang, H. Mach, M. Kosinski, M. W. Washabaugh, R. Sitrin, E. Barr, *Clin. Pharmacol. Ther. (St. Louis, MO, U. S.)* **2007**, *81*, 259.

[12] P. C. A. Bruijnincx, P. J. Sadler, in Advances in Inorganic Chemistry, (Eds: E. van Rudi, D. H. Colin) Vol. 61, Academic Press **2009** 1.

[13] M. A. Jakupec, M. Galanski, V. B. Arion, C. G. Hartinger, B. K. Keppler, *Dalton Trans.* **2008**, *183*.

[14] F. Gao, H. Chao, F. Zhou, Y.-X. Yuan, B. Peng, L.-N. Ji, *J. Inorg. Biochem.* **2006**, *100*, 1487.

[15] C. Y. Zhou, J. Zhao, Y. B. Wu, C. X. Yin, P. Yang, *J. Inorg. Biochem.* **2007**, *10*, 101.

[16] A. Guida, M. H. Lhouty, D. Tichit, F. Figueras, P. Geneste, *Appl. Catal., A* **1997**, *164*, 251.

[17] V. V. Lipson, S. M. Desenko, V. V. Borodina, M. G. Shirobokova, *Chem. Heterocycl. Compd.* **2007**, *43*, 1544.

[18] A. Z. Sayed, M. S. Aboul-Fetouh, H. S. Nassar, *J. Mol. Struct.* **2012**, *1010*, 146.

[19] P. Kaswan, K. Pericherla, D. Purohit, A. Kumar, *Tetrahedron Lett.* **2015**, *56*, 549.

[20] W. M. Motswainyana, M. O. Onani, *Inorg. Chem. Commun.* **2012**, *24*, 221.

[21] W. M. Motswainyana, M. O. Onani, A. M. Madiehe, M. Saibu, *Bioorg. Med. Chem. Lett.* **2014**, *24*, 1692.

[22] S. D. Cummings, R. Eisenberg, *J. Am. Chem. Soc.* **1996**, *118*, 1949.

[23] J. Luo, Y. Liu, Q. Chen, D. Shi, Y. Huang, J. Yu, Y. Wang, Z. Zhang, G. Lei, W. Zhu, *Dalton Trans.* **2013**, *42*, 1231.

[24] X. Chen, K. M. Engle, D. H. Wang, J. Q. Yu, *Angew. Chem. Int. Ed.* **2009**, *48*, 5094.

[25] N. R. F. B. N. Meyer, J. E. Putnam, L. B. Jacobsen, D. E. Nichols, J. L. McLaughlin, *Planta Med.* **1982**, *45*, 31.

[26] J. B. Mangrum, N. P. Farrell, *Chem. Commun.* **2010**, *46*, 6640.

[27] J. Zhao, S. Gou, Y. Sun, L. Fang, Z. Wang, *Inorg. Chem.* **2012**, *51*, 10317.

[28] C. Tu, X. Wu, Q. Liu, X. Wang, Q. Xu, Z. Guo, *Inorg. Chim. Acta* **2004**, *357*, 95.

[29] I. Huguet Ana, S. Máñez, J. Alcaraz María, *Z. Naturforsch. C* **1990**, *45*, 19.

[30] S. Bi, T. Zhao, Y. Wang, H. Zhou, B. Pang, T. Gu, *Spectrochim. Acta, Part A* **2015**, *150*, 921.

[31] A. Karaküçük-İyidoğan, D. Taşdemir, E. E. Oruç-Emre, J. Balzarini, *Eur. J. Med. Chem.* **2011**, *46*, 5616.

[32] C. G. Ricci, P. A. Netz, *J. Chem. Inf. Model.* **2009**, *49*, 1925.

[33] D. R. Kester, R. M. Pytkowicx, *Limnol. Oceanogr.* **1967**, *12*, 243.

[34] Ö. Tarı, F. Gümüş, L. Açık, B. Aydın, *Bioorg. Chem.* .

[35] P. A. Miroslava Požgajová, Anna Trakovická, **2015**, 18, 49.

[36] E. I. M. J. Moshi, J. J. Magadula, D. F. Otieno, A. Weisheit, P. K. Mbabazi, R. S. O. Nondo, *Tanzan. J. Health Res.* **2010**, *12*, 1.

[37] S. Badodi, F. Baruffaldi, M. Ganassi, R. Battini, S. Molinari, *Cell Cycle* **2015**, *14*, 1517.

[38] D. Sinha, A. K. Tiwari, S. Singh, G. Shukla, P. Mishra, H. Chandra, A. K. Mishra, *Eur. J. Med. Chem.* **2008**, *43*, 160.

[39] C. Shiju, D. Arish, N. Bhuvanesh, S. Kumaresan, *Spectrochim. Acta, Part A* **2015**, *145*, 213.

[40] G. Gliemann, *Ber. Bunsen. Phys. Chem* **1985**, *89*, 99.

[41] D. Kovala-Demertzi, A. Papageorgiou, L. Papathanasis, A. Alexandratos, P. Dalezis, J. R. Miller, M. A. Demertzis, *Eur. J. Med. Chem.* **2009**, *44*, 1296.

[42] M. Azam, Z. Hussain, I. Warad, S. I. Al-Resayes, M. S. Khan, M. Shakir, A. Trzesowska-Kruszynska, R. Kruszynski, *Dalton Trans.* **2012**, *41*, 10854.

[43] R. A. Haque, P. O. Asekunowo, M. R. Razali, *Transition Met. Chem.* **2014**, *39*, 281.

[44] Q.-X. Liu, H.-L. Li, X.-J. Zhao, S.-S. Ge, M.-C. Shi, G. Shen, Y. Zang, X.-G. Wang, *Inorg. Chim. Acta* **2011**, *376*, 437.

[45] R. A. Haque, S. Y. Choo, S. Budagumpi, M. A. Iqbal, A. Al-Ashraf Abdullah, *Eur. J. Med. Chem.* **2015**, *90*, 82.

[46] C.-H. Li, J.-H. Jiang, X. Li, L.-M. Tao, S.-X. Xiao, H.-W. Gu, H. Zhang, C. Jiang, J.-Q. Xie, M.-N. Peng, L.-L. Pan, X.-M. Xia, Q.-G. Li, *RSC Adv.* **2015**, *5*, 94267.

[47] P. Thakor, J. B. Mehta, R. R. Patel, D. D. Patel, R. B. Subramanian, V. R. Thakkar, *RSC Adv.* **2016**, *6*, 48336.

[48] D. R. Graham, L. E. Marshall, K. A. Reich, D. S. Sigman, *J. Am. Chem. Soc.* **1980**, *102*, 5419.

[49] A. Lever, D. Brown, A. Webster, H. Thomas, *Lancet* **1984**, *324*, 1062.

[50] S. C. Karad, V. B. Purohit, D. K. Raval, P. N. Kalaria, J. R. Avalani, P. Thakor, V. R. Thakkar, *RSC Adv.* **2015**, *5*, 16000.

[51] J. F. Fisher, S. O. Meroueh, S. Mobashery, *Chem. Rev.* **2005**, *105*, 395.

[52] J. Zhang, X. Zhu, A. Zhong, W. Jia, F. Wu, D. Li, H. Tong, C. Wu, W. Tang, P. Zhang, L. Wang, D. Han, *Org. Electron.* **2018**, *42*, 153.

[53] M. Monajjemi, F. Mollaamin, *J. Cluster Sci.* **2012**, *23*, 259.

[54] F. A. Tanious, D. Ding, D. A. Patrick, C. Bailly, R. R. Tidwell, W. D. Wilson, *Biochemistry* **2000**, *39*, 12091.

[55] J. M. Kelly, M. J. Murphy, D. J. McConnell, C. OhUigin, *Nucleic Acids Res.* **1985**, *13*, 167.

[56] J. M. Kelly, A. B. Tossi, D. J. McConnell, C. OhUigin, *Nucleic Acids Res.* **1985**, *13*, 6017.

[57] R. Indumathy, S. Radhika, M. Kanthimathi, T. Weyhermuller, B. Unni Nair, *J. Inorg. Biochem.* **2007**, *101*, 434.

[58] J. Liu, W. Zheng, S. Shi, C. Tan, J. Chen, K. Zheng, L. Ji, *J. Inorg. Biochem.* **2008**, *102*, 193.

[59] C. N. N'Soukpoé-Kossi, C. Descôteaux, É. Asselin, H.-A. Tajmir-Riahi, G. Bérubé, *DNA Cell Biol.* **2007**, *27*, 101.

[60] H. Soori, A. Rabbani-Chadegani, J. Davoodi, *Eur. J. Med. Chem.* **2015**, *89*, 844.

[61] G. Giaccone, *Drugs* **2000**, *59*, 9.

[62] B. Rosenberg, L. Vancamp, J. E. Trosko, V. H. Mansour, *Nature* **1969**, *222*, 385.

[63] W. D. Wilson, L. Ratmeyer, M. Zhao, L. Strekowski, D. Boykin, *Biochemistry* **1993**, *32*, 4098.

[64] A. Tarushi, K. Lafazanis, J. Kljun, I. Turel, A. A. Pantazaki, G. Psomas, D. P. Kessissoglou, *J. Inorg. Biochem.* **2013**, *121*, 53.

[65] G. Psomas, *J. Inorg. Biochem.* **2008**, *102*, 1798.

[66] J. Kljun, I. Bratsos, E. Alessio, G. Psomas, U. Repnik, M. Butinar, B. Turk, I. Turel, *Inorg. Chem.* **2013**, *52*, 9039.

[67] K. G. Samper, S. C. Marker, P. Bayón, S. N. MacMillan, I. Keresztes, Ò. Palacios, J. J. Wilson, *J. Inorg. Biochem.* **2017**, *174*, 102.

[68] Y. Zhang, T. Li, Q. Teng, *Bull. Chem. Soc. Ethiop.* **2009**, *23*, 77.

[69] M. M. G. Rabindra, *London J. Prim. Care* **2010**, *3*, 58.

[70] S. Gama, I. Rodrigues, F. Marques, E. Palma, I. Correia, M. F. N. N. Carvalho, J. C. Pessoa, A. Cruz, S. Mendo, I. C. Santos, F. Mendes, I. Santos, A. Paulo, *RSC Adv.* **2014**, *4*, 61363.

[71] R. Krikavova, J. Vanco, Z. Travnicek, R. Buchtik, Z. Dvorak, *RSC Adv.* **2016**, *6*, 3899.

[72] A. Samanta, G. K. Ghosh, I. Mitra, S. Mukherjee, J. C. Bose, K. S. Mukhopadhyay, W. Linert, S. C. Moi, *RSC Adv.* **2014**, *4*, 43516.

[73] C. Icsel, V. T. Yilmaz, Y. Kaya, H. Samli, W. T. A. Harrison, O. Buyukgungor, *Dalton Trans.* **2015**, *44*, 6880.

[74] Y.-G. Sun, D. Sun, W. Yu, M.-C. Zhu, F. Ding, Y.-N. Liu, E.-J. Gao, S.-J. Wang, G. Xiong, I. Dragutan, V. Dragutan, *Dalton Trans.* **2013**, *42*, 3957.

[75] K. Mitra, U. Basu, I. Khan, B. Maity, P. Kondaiah, A. R. Chakravarty, *Dalton Trans.* **2014**, *43*, 751.

SUPPORTING INFORMATION

Additional Supporting Information may be found online in the supporting information tab for this article.

How to cite this article: Lunagariya MV, Thakor KP, Waghela BN, Pathak C, Patel MN. Design, synthesis, pharmacological evaluation and DNA interaction studies of binuclear Pt(II) complexes with pyrazolo[1,5-a]pyrimidine scaffold. *Appl Organometal Chem*. 2018;e4222. https://doi.org/10.1002/aoc.4222